International Geology Review

ISSN: (Print) (Online) Journal homepage: https://www.tandfonline.com/loi/tigr20

New evidence for Jurassic continental rifting in the northern Sanandaj Sirjan Zone, western Iran: the Ghalaylan seamount, southwest Ghorveh

Hossein Azizi, Fatemeh Nouri, Robert J. Stern, Marie Azizi, Federico Lucci, Yoshihiro Asahara, Mohammad Hossein Zarinkoub & Sun Lin Chung

To cite this article: Hossein Azizi, Fatemeh Nouri, Robert J. Stern, Marie Azizi, Federico Lucci, Yoshihiro Asahara, Mohammad Hossein Zarinkoub & Sun Lin Chung (2020) New evidence for Jurassic continental rifting in the northern Sanandaj Sirjan Zone, western Iran: the Ghalaylan seamount, southwest Ghorveh, International Geology Review, 62:13-14, 1635-1657, DOI: 10.1080/00206814.2018.1535913

To link to this article: https://doi.org/10.1080/00206814.2018.1535913

INTERNATIONAL GEOLOGY REVIEW
2020, VOL. 62, NOS. 13–14, 1635–1657
https://doi.org/10.1080/00206814.2018.1535913

Taylor & Francis
Taylor & Francis Group

ARTICLE

New evidence for Jurassic continental rifting in the northern Sanandaj Sirjan Zone, western Iran: the Ghalaylan seamount, southwest Ghorveh

Hossein Azizi [a], Fatemeh Nouri[a], Robert J. Stern[b], Marie Azizi[c], Federico Lucci[d], Yoshihiro Asahara[e], Mohammad Hossein Zarinkoub[f] and Sun Lin Chung[g,h]

[a]Mining Department, Faculty of Engineering, University of Kurdistan, Sanandaj, Iran; [b]Geosciences Department, University of Texas at Dallas, Richardson, TX, USA; [c]Earth Sciences Department, Faculty of Basic Sciences, University of Kurdistan, Sanandaj, Iran; [d]Dipartimento di Scienze, Università Roma Tre, Roma, Italy; [e]Department of Earth and Environmental Sciences, Graduate School of Environmental Studies, Nagoya University, Nagoya, Japan; [f]Department of Geology, Faculty of Sciences, Birjand University, Birjand, Iran; [g]Institute of Earth Sciences, Academia Sinica, Taipai 11529, Taiwan; [h]Department of Geosciences, National Taiwan University, P.O. Box 13-318, Taipai 10617, Taiwan

ABSTRACT

We address the growing controversy about the tectonic setting in which Jurassic magmatism of Iran occurred: arc or continental rift. In the Ghorveh area of the northern Sanandaj Sirjan zone (SaSZ), the Ghalayan metabasites are interlayered with marble and schist and locally cut by acidic dikes. Zircon U-Pb dating of the metabasitic rocks shows that these crystallized at ca. 145–144 Ma ago in the Late Jurassic (Tithonian). This complex was metamorphosed in the lower greenschist facies, however, some protolithic structures such as pillow lava and primary minerals are preserved. The metabasites are tholeiites with low SiO_2 (45.6–50.5 wt.%), moderate Al_2O_3 (11.3–17.0 wt.%), and high TiO_2 (0.7–2.9 wt.%) and Fe_2O_3 (9.4–14.1 wt.%). The Ghalayan metabasites are enriched in Light rare earth elements (LREEs) without significant Nb, Ta, Pb, Sr and Ba anomalies, similar to modern continental intra-plate tholeiitic basalts such as Afar and East African rifts. The Ghalaylan metabasites show wide ranges for $^{87}Sr/^{86}Sr_{(i)}$ (0.7039–0.7077) and positive $\varepsilon_{Nd}(t)$ values (+0.1 to +4.6). These isotopic compositions are similar to those expected for slightly depleted subcontinental lithospheric mantle sources. Independently built discrimination diagrams indicate an intra-continental rifting regime for the source of Jurassic metabasites in the northern SaSZ. Geochemical and tectonic evidence suggests that rifting or a mantle plume was responsible for volcanic activity in the Upper Jurassic SaSZ. Considering the variation of ages of basaltic volcanism along the SaSZ, we suggest that Ghalayan basaltic magmatism reflected a submarine volcano that formed as part of the late stage continental rift, similar to Afar in the East African Rift system. Our results indicate that an extensional tectonic regime dominated SaSZ tectonics in the Middle to Late Jurassic.

ARTICLE HISTORY
Received 30 July 2018
Accepted 6 October 2018

1. Introduction

It is important to know when the SW Eurasia became a convergent margin, and Jurassic igneous activity in the Sanandaj Sirjan zone (SaSZ) of NW Iran is critical for solving this problem. In particular, SaSZ magmatic activity from Middle Jurassic to Early Cretaceous (187–143 Ma; e.g. Bayati *et al*. 2017) is considered by many authors as a consequence of Neo-Tethys convergence and subduction (e.g. Stöcklin and Nabavi 1973; Berberian and Berberian 1981; Berberian *et al*. 1982; Mohajjel *et al*. 2003; Ghasemi and Talbot 2006; Davoudian *et al*. 2008; Shahbazi *et al*. 2010, 2014; Mahmoudi *et al*. 2011; Aliani *et al*. 2012; Mohajjel and Fergusson 2014; Moinevaziri *et al*. 2015). However, the significance of these Jurassic magmatic rocks is increasingly debated. Azizi *et al*. (2018) studied the Upper Jurassic mafic Panjeh complex in the Songhor-Ghorveh area and suggested an alternative geodynamic scenario dominated by continental rifting/mantle-plume tectonics. This interpretation was supported by the regional synthesis of Azizi and Stern (submitted), who noted that Jurassic SaSZ magmatism varies systematically from oldest (177 Ma) in the SE and youngest (144 Ma) in the NW, younging from SE to NW. This behaviour is more consistent with a propagating rift than an arc, indicating that SaSZ igneous activity migrated around 600 km during a ~ 35 Ma interval at 17–20 mm yr^{-1}.

Disagreement about whether Jurassic SaSZ igneous activity occurred at a convergent plate margin above a subduction zone or at a continental rift can be called 'The Jurassic SaSZ controversy'. This controversy needs to be resolved. Here, we expand on our previous studies of Panjeh complex intrusive rocks in the Songhor-Ghorveh area (e.g. Hosseiny 1999; Azizi *et al*. 2015a, 2018; see references therein) and report new results on this voluminous magmatic

CONTACT Hossein Azizi azizi1345@gmail.com Mining Department, Faculty of Engineering, University of Kurdistan, Sanandaj, Iran

sequence. In this paper, we present systematic whole rock geochemistry, Sr–Nd isotopes and zircon U–Pb geochronology of low-grade metabasites outcropping near the Ghalaylan village, focusing on (i) the age of basaltic magmatism, (ii) magma genesis and (iii) understanding the tectonic setting of basaltic magmatism. The results are used to improve our understanding of the northern SaSZ during the Late Jurassic. We suggest that the Ghalaylan basalts together with part of the coeval neighbourhood mafic complexes of Taghiabad, Kangareh (Azizi *et al*. 2015a) and Panjeh (Azizi *et al*. 2018) provide further evidence in support of a continental rifting event affecting the Cadomian continental crust of Iran.

2. Geological setting

Identification of the Sanandaj Sirjan Zone as a discrete geological terrane was introduced by Stöcklin (1968). The SaSZ is 50–100 km wide and approximately 800 km long and tectonically bounded by the Zagros suture zone in the SW (Figure 1(a)) and the Urumieh Dokhtar magmatic arc (UDMA) in the NE (Stöcklin and Nabavi 1973; Berberian and Berberian 1981; Berberian *et al*. 1982; Alavi 1994; Mohajjel *et al*. 2003; Golonka 2004; Ghasemi and Talbot 2006; Davoudian *et al*. 2008; Chiu *et al*. 2013; Mohajjel and Fergusson 2014). The SaSZ marks the SW margin of the Iranian micro-continent (Hassanzadeh *et al*. 2008; Azizi *et al*. 2016). The SaSZ also separates Late Cretaceous Zagros ophiolites into Inner and Outer Belts (Moghadam and Stern 2015).

The SaSZ is characterised by regionally metamorphosed and deformed rocks that are spatially associated with abundant Jurassic intrusions and volcanic rocks (Berberian and Berberian 1981; Sepahi and Athari 2006; Ahmadi-Khalaji *et al*. 2007; Sepahi 2008; Azizi *et al*. 2011; Maanijou *et al*. 2011; Aliani *et al*. 2012; Azizi and Asahara 2013; Deevsalar *et al*. 2014, 2017; Mohajjel and Fergusson 2014; Yajam *et al*. 2015). Cadomian (~550 Ma) basement – which makes up most of the Iranian crust – outcrops in much of the SaSZ (Stöcklin and Nabavi 1973; Berberian and Berberian 1981; Berberian *et al*. 1982; Mohajjel *et al*. 2003; Golonka 2004; Ghasemi and Talbot 2006; Davoudian *et al*. 2008; Hassanzadeh *et al*. 2008; Malek-Mahmoudi *et al*. 2017; Shabanian *et al*. 2017).

The SaSZ is divided into northern and southern sections (Eftekharnejad 1981: Figure 1(a)). The southern SaSZ abundantly exposes Triassic metamorphic rocks (Ahmadipour *et al*. 2003; Sheikholeslami *et al*. 2008; Hosseini *et al*. 2009; Shabanian *et al*. 2009; Izadyar *et al*. 2013) with minor Jurassic calc-alkaline igneous rocks (Arvin *et al*. 2007; Fazlnia *et al*. 2009). The northern SaSZ locally exposes Cadomian basement (Moghadam *et al*. 2015, 2016; Honarmand *et al*. 2017; Shabanian *et al*. 2017; Badr *et al*. 2018) but is dominated by the Jurassic metamorphic complex (Baharifar *et al*. 2004) intruded by Late Jurassic magmatic rocks (Berberian *et al*. 1982; Esmaeily *et al*. 2005; Sepahi and Athari 2006; Arvin *et al*. 2007; Torkian *et al*. 2008; Mazhari *et al*. 2009; Shahbazi *et al*. 2010, 2014; Azizi *et al*. 2011, 2015a, 2015b, 2016; Azizi and Asahara 2013; Zhang *et al*. 2018). A Middle Triassic to Upper Jurassic volcano-sedimentary metamorphic complex is widely exposed in the northern SaSZ (Mohajjel and Fergusson 2000; Mohajjel *et al*. 2003). N-SaSZ Mesozoic sequences are characterized by volcanic (basalts, andesitic basalts and andesites), subvolcanic (dolerites and microdiorites), volcaniclastic (tuffs, agglomerate and hyaloclastic breccia) rocks interbedded with marbles, black-shales, slates and metasandstones defining a marine basin built on continental (Cadomian) crust. The N-SaSZ complex is unconformably overlain by Cretaceous limestones (Eftekharnejad 1981; Kazmin *et al*. 1986; Alavi 1994; Hosseiny 1999; Baharifar *et al*. 2004). Upper Jurassic greenschist to locally amphibolite metamorphism is documented (Mohajjel *et al*. 2003; Baharifar *et al*. 2004; Nasr-Esfahani and Ziaei 2007; Davoudian *et al*. 2008). Various studies (e.g. Eftekharnejad 1981; Kazmin *et al*. 1986; Alavi 1994; Ghasemi and Talbot 2006) identified calc-alkaline to tholeiitic signatures for these Jurassic volcanic rocks, suggesting their genesis above a subduction zone in an active continental margin. However, in the last decade alternative scenarios have been proposed such as: (i) immature island arc, (ii) back arc basin, (iii) thinning of continental lithosphere and/or mantle upwelling and (iv) continental/intraplate rifting due to mantle plume (e.g. Hosseiny 1999; Mousivand *et al*. 2012; Nasr-Esfahani 2012; Azizi and Asahara 2013; Rajabzadeh and Esmaeili 2014; Ahmadi-Khalaji *et al*. 2015; Hunziker *et al*. 2015; Zarasvandi *et al*. 2015; Azizi *et al*. 2015a, 2015b, 2018; Shakerardakani *et al*. 2018). Which is the most appropriate tectonic setting for these igneous rocks?

3. Local geology and field observation

Basement of the Ghorveh region (Figures 1(a,b and 2(a)) consists of the Hamadan-Ghorveh metamorphic complex (Hosseiny 1999; Baharifar *et al*. 2004; Azizi and Asahara 2013) made of slate, phyllite, schist, marble, and quartzite interbedded with submarine metavolcanic rocks. Fossils define a depositional age from Late Triassic to Middle Jurassic (Hosseiny 1999) in a marine environment. Near the city of Sanandaj, the metamorphic complex is unconformably overlain by unmetamorphosed Cretaceous sedimentary rocks (Hosseiny 1999; Mohajjel *et al*. 2003; Mohajjel and Fergusson

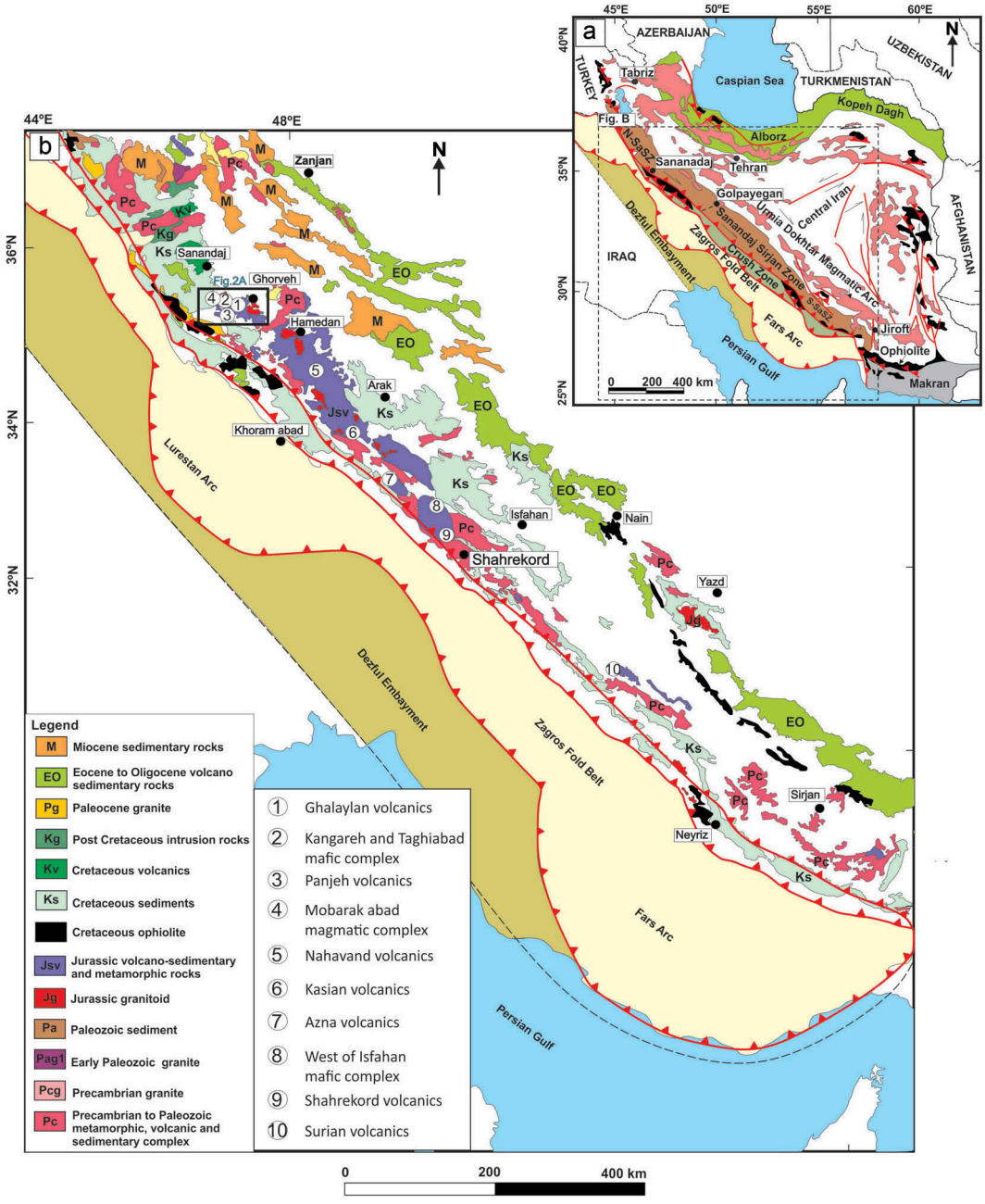

Figure 1. (a) Simplified geological map of Iran (modified from Stöcklin 1968). (b) Simplified geological map of northern Sanandaj Sirjan zone (N-SaSZ), which shows the bodies that trend parallel to Zagros suture zone in western Iran (modified from Stöcklin 1968).

2014) (Figure 2), indicating that Hamadan-Ghorveh metamorphism occurred in Middle to Late Jurassic time (Hosseiny 1999; Azizi *et al*. 2015a). In the Middle Jurassic to Early Cretaceous (ca. 180–140 Ma) the Hamadan–Ghorveh metamorphic complex was intruded by both granitoid and gabbroic bodies (Azizi *et al*. 2011, 2015a, 2015b, 2018; Azizi and Asahara 2013), and most of this magmatic complex is also covered by Cretaceous sedimentary rocks (Hosseiny 1999; Azizi *et al*. 2015a, 2015b, 2018). The absence of Precambrian basement near the Hamedan–Ghorveh metamorphic complex has been interpreted by Azizi *et al*. (2015a), (2015b)) as evidence that an intra-oceanic island arc collided and metamorphosed during the Late Cimmerian orogeny. Large volume of mafic rocks widely distributed in the Kangareh, Taghiabad and Ghalylan area (Figure 2(a)).

The Ghalaylan metabasaltic complex outcrops near the village of Ghalaylan (Figures 2(a,b)) interbedded with the metasedimentary rocks of the Hamedan–

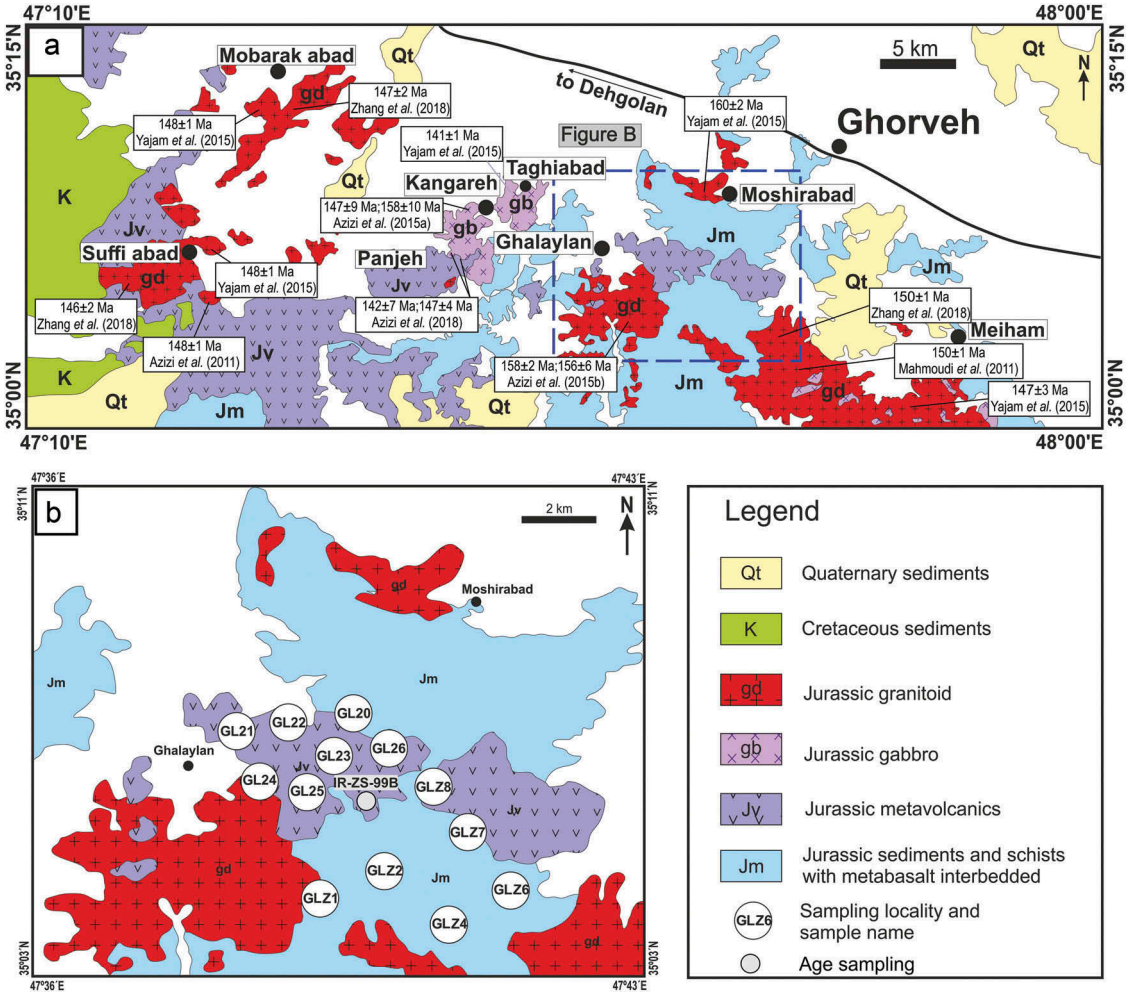

Figure 2. (a) Simplified geological map of the Ghorveh region with radiometric ages for the igneous rocks in this area (modified from Hosseiny 1999). Dashed line shows the study area, and sampling locations are indicated (b).

Ghorveh metamorphic complex. In the study area, the metasediments are mainly characterized by (i) foliated marbles (Figure 3(a)), (ii) meta-chert ribbons along the marble foliation (Figure 3(b)), and (iii) minor metapelites (Figure 3(c)) interbedded within the metabasalts and the marbles.

Outcropping Ghalaylan metabasaltic rocks are mafic flows and pillow lavas always interbedded with marbles, as undeformed basalts or as greenstone to foliated greenschist rocks (Figure 3(d)). Greenschist-facies metamorphism is revealed by diffuse recrystallization of secondary chlorite and epidote (Hosseiny 1999; Shaikh Zakariaei and Monsef 2010; Moinevaziri *et al*. 2015; Azizi *et al*. 2015a, 2015b). Metabasaltic layers interbedded with marbles range from a few centimeters up to few meters thick (Figures 3(e,f)). Locally, it is possible to recognize also basaltic patches and bombs embedded in marbles (Figure 3(f)). The overall sense of the Ghalaylan metabasaltic rocks and associated marbles is that these are remnants of an Upper Jurassic submarine volcano and its sedimentary apron. Intrusive gabbro and granite of similar age define the heart of the volcano (Yajam *et al*. 2015; Azizi *et al*. 2018; Zhang *et al*. 2018).

4. Petrography

Ghalaylan metabasaltic rocks consist mainly of plagioclase, clinopyroxene and amphibole (Figures 4(a, b)). Original porphyry and intersertal textures (Figures 4(b–d) are locally preserved. Plagioclase and pyroxene phenocrysts are partially preserved (Figures 4(c,d)). Groundmass comprises elongated amphibole and plagioclase with subordinate titanite and Fe-Ti oxides. Plagioclase phenocrysts with euhedral to subhedral shape are replaced by epidote, calcite and albite (Figure 4(e)). Clinopyroxene is an early crystallizing phase replaced by actinolite (Figure 4(e,f)).

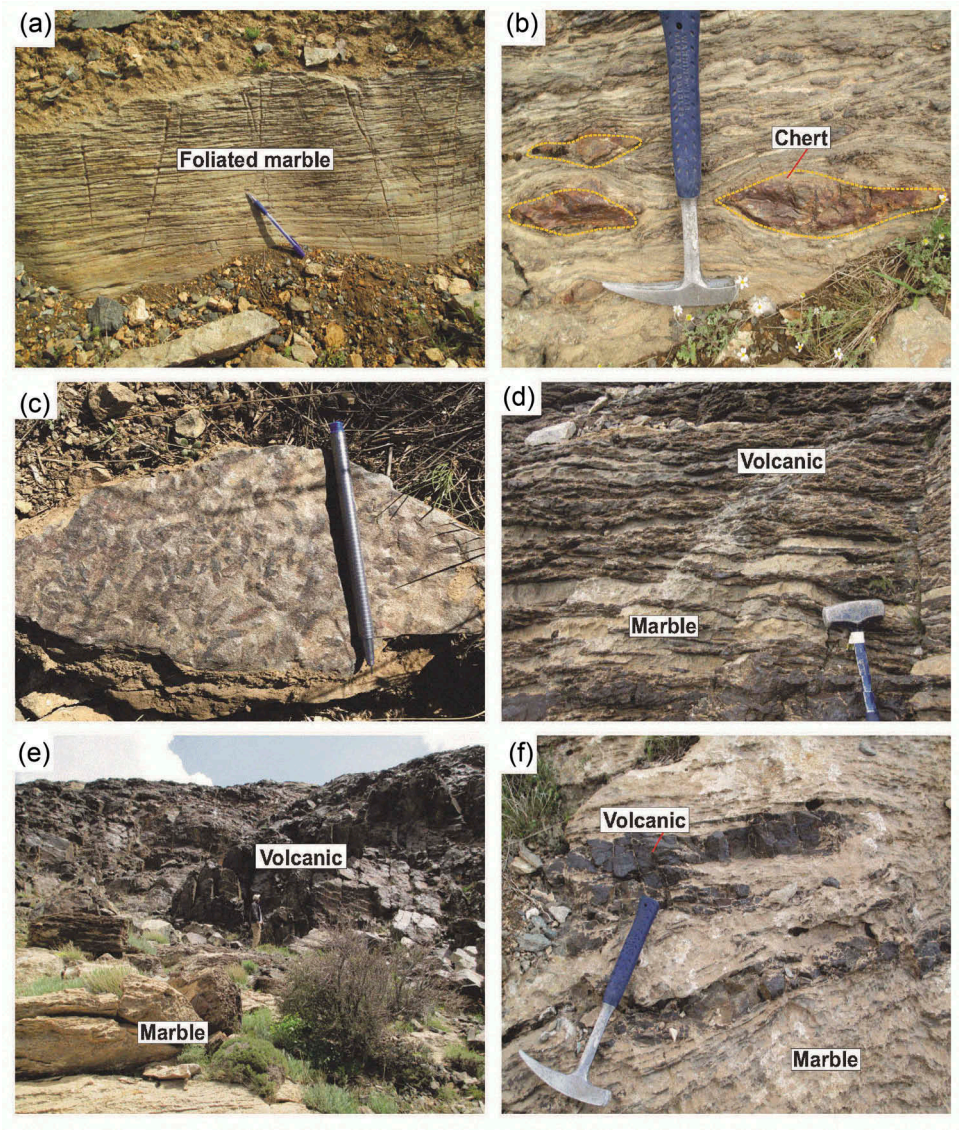

Figure 3. (a) Mylonitized (foliated) marbles with stretching lineation. (b) Cherts forming small boudins in marble, elongated along stratification. (c) Andalusite porphyroblasts in metapelites. (d) Volcaniclastic layers in marble. (e) Mafic lava flows on top of marble. Lavas are affected by low grade metamorphism, ranging from relatively undeformed basalt to greenstone or foliated greenschist. (f) Dimensions of metavolcanic layers scattered throughout the metasedimentary sequence are highly variable. Some basaltic patches found in the marble are undeformed.

5. Analytical techniques

5.1. Zircon U-Pb dating

Zircons for U-Pb dating were separated from basalt sample IR-Z-S-99B using conventional magnetic (neodymium magnet) and bromoform ($CHBr_3$) heavy liquid separation techniques. Because of the very low amount of zircon crystals in these basaltic rocks about 2 kg of the sample was crushed. Obtained zircon were handpicked and then placed on a glass side. After polishing, backscattered electron (BSE) and cathodoluminescence (CL) images of zircon were obtained at the Institute of Earth Sciences at Beijing University to identify flawless zircon crystals, to investigate their internal textures/domains and to define shooting points for dating. U-Pb ages were obtained with a laser ablation (LA, New Wave UP213 system) inductively coupled mass spectrometer (ICPMS Agilent 7500s quadrupole) at the Department of Geosciences, National Taiwan University. U-Pb analyses were performed using helium (He) as carrier gas to improve transport efficiency (Eggins *et al.* 1998; Günther and Heinrich 1999; Jackson *et al.* 2004). Common Pb correction was applied following

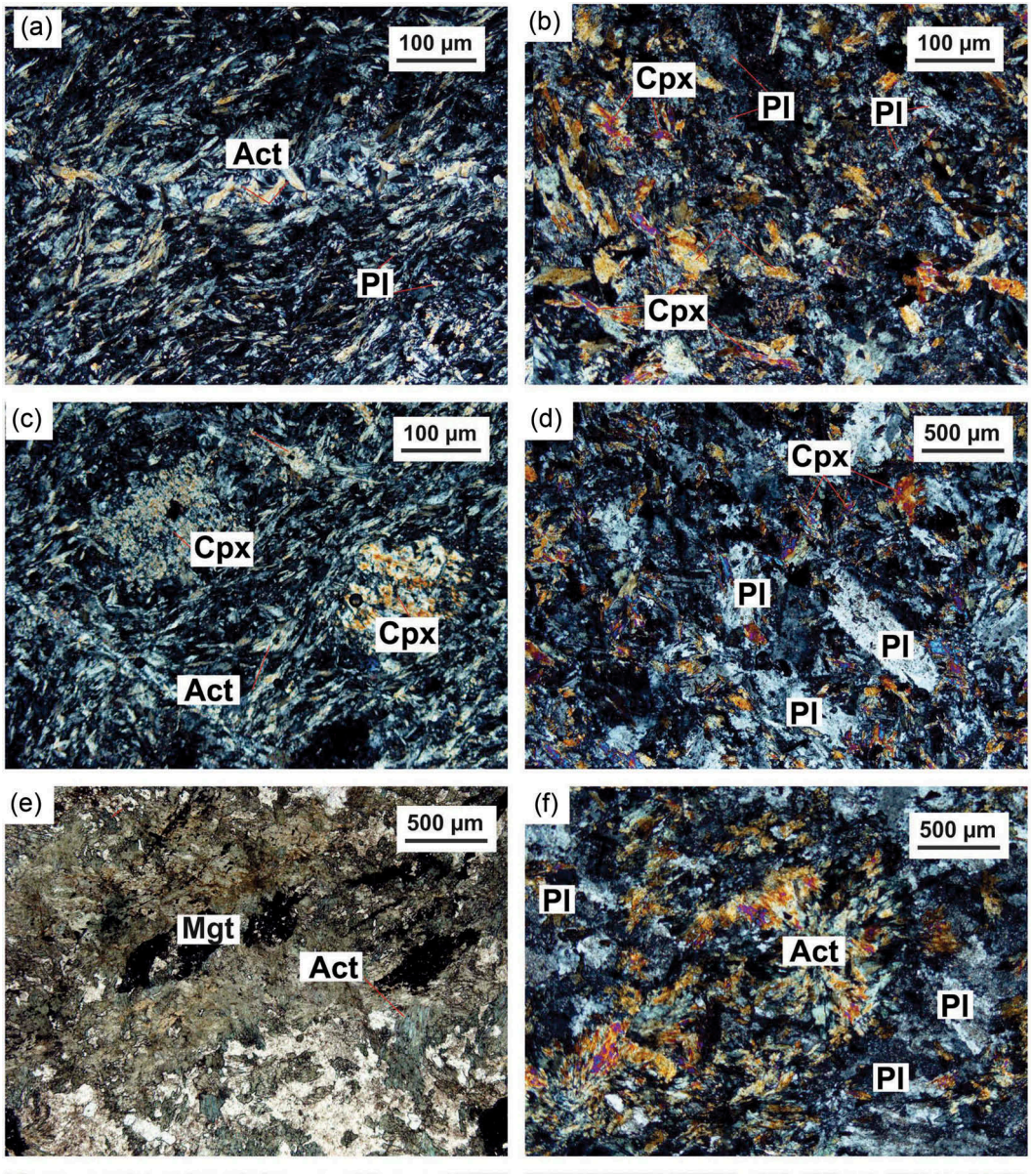

Figure 4. Thin section images of Ghalaylan metamafic rocks. (a) Basaltic layers are metamorphosed and are mostly foliated due to mineral lineation. (b) Metabasalts consist mainly of plagioclase, clinopyroxene and amphibole. (c, d) Metabasalts are porphyritic with abundant plagioclase and pyroxene phenocrysts which are usually set in an intersertal groundmass. (e) Plagioclase (Pl) are euhedral to subhedral, plagioclase phenocrysts are moderately saussuritized. (e, f) Clinopyroxene (Cpx) is colorless to brown, it is an early crystallizing phase that is partially replaced by actinolite. Abbreviations: Cpx = Clinopyroxene, Pl = Palgiocalse, Act = Actonilite. Tr = tremolite (abbreviation from Whitney and Evans 2010).

the in Stacey and Kramers (1975). The ISOPLOT v.4.15 program (Ludwig 2012) was used for calculating the Concordia and ages, statistics, and for constructing plots.

5.2. Whole rock geochemistry and Sr-Nd isotopes

A total of 13 basaltic rocks were selected for whole-rock chemical and Sr-Nd isotope analyses (Figure 2(b)). Analyses were carried out following procedures and workflow presented in Azizi *et al.* (2015a).

Major element concentrations of the 13 samples were measured by conventional X-ray fluorescence (XRF) method using a ZSX Primus II (Rigaku Co., Japan) at Nagoya University, Japan. Glass-beads for XRF analyses were prepared mixing 0.5 g of sample powder with 5.0 g of lithium tetraborate. This mixture was then melted at 1200°C for 15 min with a high-frequency bead sampler (Rigaku Co., Japan). Loss on ignition (LOI) was measured from the sample powder weight in a quartz glass beaker in the oven at 950°C for 5 hours.

For determining trace element contents and Sr-Nd isotope ratios, 100 mg of rock powder for each sample was decomposed in a covered PTFE beaker using 3 ml of HF (50%) and 0.5–1 mL $HClO_4$ (70%) at 120–140°C on a hotplate for 3 days until the powder was completely dissolved. After removing the PTFE cover, dissolved samples were dried at 140°C on a hotplate with infrared lamps for up to 2 days. After this procedure, samples were dissolved in 10 mL of 2 to 4 M HCl and the resulting solution was analyzed. Sr and Nd separations were carried out using cation-exchange resin columns (BioRad AG50W-X8, 200–400 mesh).

Trace element concentrations were analyzed using the ICP-MS (Agilent 7700x) at Nagoya University. Isotope ratios of Sr and Nd were measured by thermal ionization mass spectrometers (TIMS; a VG-Sector 54–30 and a GVI IsoProbe-T) at Nagoya University. Measured Sr and Nd isotope ratios were corrected for fractionation based on $^{86}Sr/^{88}Sr = 0.1194$ and $^{146}Nd/^{144}Nd = 0.7219$, respectively. NIST-SRM987 and JNdi-1 (Tanaka *et al*. 2000) were adopted as standards for $^{87}Sr/^{86}Sr$ and $^{143}Nd/^{144}Nd$ ratios, respectively. Averages and 1SD for isotope ratio standards, NIST-SRM987 and JNdi-1, were $^{87}Sr/^{86}Sr = 0.710244 \pm 0.000009$ (n = 11) and $^{143}Nd/^{144}Nd = 0.512113 \pm 0.00006$ (n = 9).

6. Results

6.1. Zircon U-Pb age

Zircons in the metabasite rocks are mostly subhedral transparent and colourless with some fractured and internal oscillatory zoning. Results of U-Pb analysis of zircons from sample IR-Z-S-99B (metabasite) are listed in Table 1 and shown in Figures 5(a,b). All grains have Th/U ratios higher than 0.3, confirming the magmatic origin of the zircons (Hoskin and Black 2000). After correcting for common Pb (Stacey and Kramers 1975), Isoplot software version 4.15 (Ludwig 2012) was used for age calculation. As shown in Figure 5, the obtained data define a mean age of 144.6 ± 1.9 Ma and MSWD = 1.19, consistent with the stratigraphic Jurassic age reported by Hosseiny (1999).

6.2. Whole rock geochemistry

Data for major and trace element compositions in the 13 basalts from the Ghalaylan mafic complex are presented in Table 2. Analyzed samples show mafic compositions with 45.6–50.5 wt.% SiO_2, 11.3–17.0 wt.% Al_2O_3, and 4.5–14.8 wt. % MgO with Mg# (molar $Mg/[Mg+Fe_{tot}]$) = 29–56. Sum of alkalies (Na_2O+K_2O) varies from 1.0 to 4.6 wt.% with Na_2O always higher than K_2O (mean values are 2.6 wt.% and 0.5 wt.%, respectively). High TiO_2 contents (up to 2.9 wt.%) and low Al_2O_3/TiO_2 (mean value 9.4) ratios indicate that these are not high-Mg melts or komatiites (e.g. Redman and Keays 1985; Arndt and Jenner 1986; Gao and Zhou 2013). One sample (GL-21) is primitive (10.9 wt. % MgO, 137 ppm Ni) but has unusually low TiO_2 (0.71 wt. %). This sample crops up as unusual in trace element and isotopic diagrams discussed later.

According to the total alkalies versus silica (TAS) diagram (LeMaitre *et al*. 2002), the Ghalaylan rocks fall in the basalt field (Figure 6(a)). In the K_2O vs. SiO_2 diagram (Peccerillo and Taylor 1976) the Ghalaylan samples show low-K (tholeiite) to shoshonite affinities (Figure 6(b)). On the FeO_t/MgO vs. SiO_2 diagram (Miyashiro and Shido 1975; Dilek *et al*. 2008), the Ghalaylan lavas are tholeiites (Figure 6(c)). Harker diagrams for selected major and trace elements are presented in Figures 7 and 8. SiO_2 is used to track differentiation and negatively correlates with MnO and CaO, and positively correlates with Na_2O (Figure 7). Both large ion lithophile elements (LILEs) and high field strength elements ($HFSE_S$) scatter with no appreciable correlation with silica (Figure 8).

In chondrite-normalized diagrams (Sun and McDonough 1989) the Ghalaylan complex shows highly fractionated rare earth element (REE) patterns (Figure 9(a)) with Light-REEs (LREEs) > Heavy-REEs (HREEs) as indicated by $(La/Yb)_N$ and $(Dy/Yb)_N$ ratios of 3.5–5.5 and 1.3–1.5, respectively. The same patterns are also observed for neighbour basaltic and gabbroic rocks such as Panjeh, Taghiabad and Kangareh (Figures 9(b,c)). There is no Eu anomaly ($Eu/Eu^* = [Eu_N/(Sm_N x Gd_N)^{1/2}]$; mean = 1.01, ranging 0.75–1.15) (Figures 9(a–c)). In the primitive mantle (PM)-normalized trace-element diagram (Figures 9(e–h)), the Ghalaylan basalts are generally enriched in Th, La, Ce, Nd and Ti; slight depletion of Nb-Ta-Zr-Ti is recognized only for unusual sample GL21.

In the TiO_2 vs V diagram (Figure 10(a); Shervais 1982; Reagan *et al*. 2010), the Ghalaylan samples, with Ti/V ranging 37–57, show Mid-Oceanic Ridge Basalt (MORB)-like to Oceanic Island Basalt (OIB)-like signatures. Arc-like signature is recognized only for unusual sample GL21 with $TiO_2 < 1.0$ wt.% and Ti/V = 17. In the Th/Yb vs Nb/Yb diagram (Pearce 2008), the Ghalaylan basalts plot in and above the MORB-OIB array (Figure 10(b)), falling near Enriched (E)-MORB. Elevation of points above the mantle array may reflect a subduction-modified mantle source or crustal contamination.

6.3. Sr-Nd isotope geochemistry

Sr (13 samples) and Nd (7 samples) isotope compositions for the Ghalaylan basalts are reported in Table 3. Based on U-Pb zircon age obtained in this study, the initial Sr-Nd isotope values were calculated at 145 Ma. Studied

Table 1. U-Pb isotope data for zircon grains which is determined by LA-ICP-MS.

			U-Th-Pb ratio												Age (Ma)				
					Error			Error			Error			Error	$^{206}Pb/^{238}U$ age	Error	$^{208}Pb/^{232}Th$ age		Error
Sample name	U (ppm)	Th/U	$^{207}Pb/^{235}U$ age		1σ	$^{206}Pb/^{238}U$		1σ	$^{207}Pb/^{206}Pb$		1σ	$^{208}Pb/^{232}Th$		1σ	Ma	1σ	Ma		1σ
IR-ZS-99B	Basalt																		
IR99-01	509	1.33	0.1616	±	0.0047	0.0218	±	0.0005	0.0539	±	0.0007	0.0068	±	0.0002	139	± 3	136	±	4
IR99-03	1151	2.08	0.1555	±	0.0037	0.0229	±	0.0005	0.0493	±	0.0005	0.0074	±	0.0002	146	± 3	149	±	4
IR99-04	1440	1.67	0.1677	±	0.0039	0.0233	±	0.0005	0.0522	±	0.0005	0.0073	±	0.0002	148	± 3	148	±	4
IR99-05	1876	0.88	0.1603	±	0.0037	0.0234	±	0.0005	0.0498	±	0.0005	0.0072	±	0.0002	149	± 3	145	±	4
IR99-06	1653	1.41	0.1533	±	0.0036	0.0223	±	0.0005	0.0498	±	0.0005	0.0070	±	0.0002	142	± 3	140	±	4
IR99-07	1915	0.15	0.1589	±	0.0038	0.0234	±	0.0005	0.0492	±	0.0005	0.0074	±	0.0002	149	± 3	150	±	5
IR99-08	1903	1.45	0.1605	±	0.0038	0.0225	±	0.0005	0.0518	±	0.0005	0.0071	±	0.0002	143	± 3	143	±	4
IR99-11	575	0.67	0.1549	±	0.0048	0.0227	±	0.0005	0.0494	±	0.0007	0.0077	±	0.0003	145	± 3	155	±	6
IR99-13	785	1.23	0.1666	±	0.0047	0.0222	±	0.0005	0.0543	±	0.0007	0.0073	±	0.0003	142	± 3	148	±	6
IR99-14	796	1.19	0.1587	±	0.0040	0.0222	±	0.0005	0.0519	±	0.0006	0.0077	±	0.0003	141	± 3	155	±	5
IR99-15	1008	0.85	0.1675	±	0.0044	0.0224	±	0.0005	0.0544	±	0.0006	0.0080	±	0.0003	142	± 3	161	±	6
IR99-16	1996	0.51	0.1820	±	0.0050	0.0232	±	0.0005	0.0568	±	0.0007	0.0075	±	0.0004	148	± 3	150	±	7
IR99-17	1422	0.54	0.1648	±	0.0043	0.0231	±	0.0005	0.0517	±	0.0006	0.0083	±	0.0003	147	± 3	168	±	7
IR99-18	1016	0.40	0.1523	±	0.0043	0.0224	±	0.0005	0.0493	±	0.0006	0.0083	±	0.0004	143	± 3	168	±	7

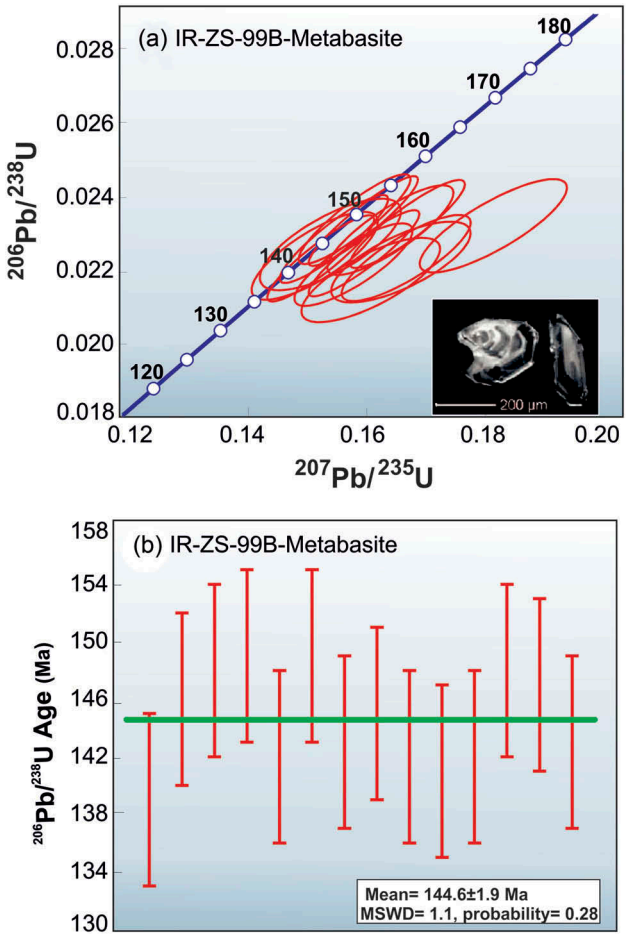

Figure 5. (a, b) Zircon U-Pb Concordia and mean 206Pb/238U age diagrams for IR-ZS-99B (metabasalt).

samples present $^{87}Sr/^{86}Sr_{(145Ma)}$ ranging 0.7039–0.7077 (mean = 0.7059) and εNd(t) ranging from +0.1 to +4.6, except for sample GL20 showing εNd(t) = −7.8 (mean = + 1.4). GL20 is especially interesting because it is geochemically similar to other OIB-like Ghalaylan basalts. Nd model ages (T_{DM1}; DePaolo and Wasserburg 1976) are 0.8–1.1 Ga for most of the Ghalaylan basalts. Sample GL20, showing a negative εNd(t) value (−7.8), plots in the Enriched Mantle quadrant in the field of Continental Flood Basalts (i.e. Hawkesworth *et al*. 1983; Philpotts and Ague 2009). Nd model age (T_{DM1}; DePaolo and Wasserburg 1976) is 2.1 Ga for GL20 sample.

7. Discussion

Geochronological, geochemical and isotope ratio data for the Ghalaylan metabasalts are discussed below. We first discuss the tectonic affinities of Ghalayan metabasalts, then the evolution of the magma, and finally the implications of these results for resolving the Jurassic SaSZ controversy.

7.1. Tectonic affinities

The Ghalaylan mafic complex is composed of Late Jurassic/Early Cretaceous (ca.145 Ma) unmetamorphosed to greenschist facies basalts and associated intrusive rocks (Figure 6(a)) showing a low-K to medium-K character (Figure 6(b)) with tholeiitic signatures (Figure 6(c)). Ghalaylan REE- and trace-element patterns are graphically compared (Figures 9(a,e)) to those of (i) island arc basalts (after Buchs *et al*. 2013), (ii) back-arc basalts (BABB; Pearce *et al*. 2005; Buchs *et al*. 2013), (iii) forearc basalts (FAB; Reagan *et al*. 2010; Ishizuka *et al*. 2011), (iv) mid-ocean ridge basalts (MORB; Jenner and O'Neill 2012), and (v) ocean island basalts (OIB; Willbold and Stracke 2006; Buchs *et al*. 2013). With the exception of GL21, the Ghalaylan basalts show patterns that are most similar to OIB (Li *et al*. 2013; Ayalew *et al*. 2016).

Further evidence for the OIB-like nature of the Ghalaylan metabasalts is provided by our geochemical results. Subduction-related magmas generally contain low TiO_2, typically <1wt. % whereas OIB magmas and rift-related basalts contain significantly more TiO_2. Except for unusual sample GL21 (TiO_2: 0.71 wt. %), the Ghalaylan basalts contain OIB-like abundances (1.2–2.9 wt.%) of TiO_2. Ti/V ratios are also useful for identifying tectonic settings of magmatism. Except for unusual sample GL-21 (Ti/V: 17), the Ghalaylan basalts have Ti/V = 37–57 and plot in the region occupied by enriched MORB and OIB (Figure 10(a)). An E-MORB source is also suggested from the Th/Yb vs. Nb/Yb system (after Pearce 2008; Dilek and Furnes 2014). On this diagram (Pearce 2008), the Ghalaylan samples plot close above the MORB-OIB array (Figure 10(b)) near the composition of lower continental crust (after Pearce 2008; Buchs *et al*. 2013; Rossetti *et al*. 2017; Azizi *et al*. 2018). This suggests that Ghalaylan magmas might have interacted with continental crust material (Pearce 2008; Azizi *et al*. 2018), however this signature could also be inherited from Cadomian subcontinental lithospheric mantle that was affected by subduction-related metasomatism at ~550 Ma.

An OIB-mantle origin is also confirmed by Nb/La ratios (Peate 1997; Anh *et al*. 2011) (Figure 10(c)). Condie (1999) used La/Nb ratios and Ni content for #Mg: 40 (Ni_{40}) to distinguish basaltic rocks in different tectonic setting. Arc basalts are characterized by low Ni_{40} (less than 40 ppm) and higher La/Nb (>1.6), whereas MORB and oceanic plateau basalts (OIB) have higher Ni_{40} and lower La/Nb. The basaltic rocks of the Ghalaylan area mainly have high Ni_{40} (40–180 ppm) and low La/Nb and are clearly distinguished from arc basalts on this basis (Figure 10(c)). Finally, on the La-Y-Nb (Cabanis and Lecolle 1989) diagram (Figure 10(d)), most samples plot in the continental rift field.

Table 2. Whole rocks composition of Ghalaylan complex.

Sample	GL20	GL21	GL22	GL23	GL24	GL25	GL26	GLZ1	GLZ2	GLZ4	GLZ6	GLZ7	GLZ8
Rock type	Basalt	Basalt	Basalt	Basalt	Basalt	Basalt	Basalt	Basalt	Basalt	Basalt	Basalt	Basalt	Basalt
SiO_2 (wt.%)	50.45	48.69	48.49	47.85	46.63	48.18	47.61	45.66	45.62	49.30	49.95	49.78	49.97
TiO_2	1.90	0.71	1.67	1.72	2.89	1.78	1.23	1.70	1.53	2.17	1.68	1.65	1.64
Al_2O_3	15.60	13.50	14.50	14.40	13.90	14.70	11.30	16.59	15.48	17.04	16.64	14.49	14.85
Fe_2O_3	10.08	9.36	12.00	12.40	14.10	12.80	14.10	12.27	10.04	12.31	10.59	11.58	11.90
MnO	0.15	0.17	0.17	0.17	0.34	0.19	0.19	0.21	0.19	0.22	0.15	0.18	0.17
MgO	7.25	10.93	7.69	8.06	5.34	6.35	14.75	7.70	8.86	4.45	7.14	7.59	7.44
CaO	8.89	11.85	11.77	12.17	11.83	10.72	7.42	10.81	14.66	8.72	8.93	11.13	9.52
Na_2O	3.61	2.28	2.29	2.15	1.64	2.94	0.95	2.75	1.20	4.09	3.40	2.68	3.68
K_2O	0.58	0.45	0.39	0.14	1.55	0.94	0.05	0.98	0.55	0.51	0.45	0.24	0.19
P_2O_5	0.25	0.16	0.20	0.20	0.38	0.23	0.14	0.21	0.20	0.24	0.20	0.19	0.19
LOI	1.20	2.71	0.79	0.58	1.30	1.08	2.89	1.28	2.12	0.91	1.32	1.01	0.63
Total	99.96	100.81	99.96	99.84	99.90	99.91	100.63	100.16	100.45	99.97	100.46	100.51	100.17
V (ppm)	268	246	266	278	305	278	166	264	238	278	258	263	261
Sc	*	*	*	*	*	*	*	33.9	30.5	27.6	35.4	33.6	33.8
Cr	128	753	483	565	48.8	113	1321	278	388	33.5	245	350	383
Co	26.2	39.5	48.2	49.1	21.8	34.3	80.2	42.4	49.1	25.3	31.7	38.8	38.0
Ni	29.1	137	172	146	33.4	24.3	620	108	187	22.1	55.1	108	125
Cu	9.52	62.6	104	95.1	12.1	16.6	18.7	92.0	4.44	8.94	6.94	30.1	59.2
Zn	71.5	78.5	96.0	104	105	90.2	95.9	115	136	88.4	87.7	89.2	102
Ga	20.6	12.4	19.2	18.4	29.4	18.5	14.2	22.1	17.6	23.5	20.1	18.9	17.0
Rb	20.7	8.64	8.89	2.04	79.1	32.0	3.20	29.7	20.0	18.6	15.5	5.54	3.96
Sr	425	349	371	383	359	463	34.3	421	610	440	432	425	344
Y	27.8	15.5	20.9	22.0	33.0	20.9	13.4	21.8	20.3	21.1	22.4	21.9	20.5
Zr	75.9	43.3	104	99.4	155	128	58.2	108	124	131	89.3	99.1	111
Nb	16.8	2.37	10.4	10.5	21.7	15.9	5.84	7.10	7.83	9.37	7.38	7.18	7.81
Cs	2.32	0.440	0.400	0.15	1.52	1.06	0.250	0.826	0.570	0.436	1.82	0.408	0.204
Ba	111	100	99.0	30.1	192	74.6	11.5	94.1	43.6	107	132	49.4	41.1
Hf	2.74	1.45	3.23	3.14	3.90	3.73	1.81	3.04	3.30	3.50	3.11	2.93	3.06
Ta	1.16	0.26	0.790	0.81	1.29	1.14	0.480	0.679	0.658	0.849	0.768	0.608	0.618
Pb	3.61	3.08	2.38	5.85	2.57	2.17	1.36	10.0	2.74	4.55	3.95	3.95	5.66
Th	3.62	1.98	1.11	0.98	1.37	1.78	0.840	1.42	2.74	1.53	2.38	1.02	1.13
U	0.72	0.36	0.320	0.29	0.9	0.35	0.210	0.456	2.72	0.414	0.599	0.337	0.274
La	18.0	10.4	9.67	9.80	23.2	13.3	7.65	12.9	14.7	14.3	14.2	9.63	9.43
Ce	40.6	22.3	23.2	23.2	49.0	29.7	17.6	28.8	32.4	31.9	30.7	22.1	21.9
Pr	5.11	2.96	3.07	3.11	6.23	3.80	2.32	3.67	4.00	4.09	3.93	3.05	2.95
Nd	22.1	13.3	14.3	14.6	27.2	16.4	10.3	16.2	17.1	17.7	17.1	13.8	13.7
Sm	5.24	3.11	3.63	3.79	6.34	3.69	2.39	4.04	3.92	4.08	4.04	3.71	3.39
Eu	1.33	1.05	1.30	1.34	2.44	1.04	0.829	1.52	1.50	1.47	1.27	1.42	1.22
Gd	5.71	3.21	4.32	4.54	6.82	4.07	2.77	4.43	4.11	4.40	4.35	4.17	3.94
Tb	0.900	0.474	0.697	0.724	1.07	0.654	0.444	0.684	0.660	0.687	0.683	0.678	0.619
Dy	5.63	3.02	4.31	4.54	6.57	4.14	2.78	4.27	4.00	4.09	4.30	4.26	3.93
Ho	1.11	0.611	0.837	0.889	1.301	0.831	0.545	0.842	0.793	0.814	0.854	0.849	0.757
Er	3.06	1.72	2.27	2.42	3.67	2.36	1.46	2.32	2.18	2.20	2.40	2.30	2.14
Tm	0.415	0.238	0.307	0.323	0.500	0.328	0.205	0.314	0.296	0.306	0.319	0.294	0.280
Yb	2.57	1.56	1.89	2.01	3.15	2.04	1.24	1.96	1.91	1.90	2.00	1.89	1.82
Lu	0.351	0.227	0.258	0.278	0.436	0.288	0.170	0.287	0.272	0.273	0.303	0.278	0.284

* not measured

Arc-signature has been identified instead for Ghalaylan GL21 sample similar to that of Kangareh coarse-grained gabbro (146–148 Ma; Azizi *et al*. 2015a, 2018) as indicated by: (i) tholeiitic to calc-alkaline signature (Figure 6(c)); (ii) TiO_2 content <1.0 wt.% (Figures 7, 10(a)); (iii) Ti/V ratio ~20 (Figure 10(a)) typical of arc magmatism; (iv) general lower enrichments of REE and HFSE in PM-normalized diagrams (Figures 9(e,h); Sun and McDonough 1989), with negative anomalies of Nb and Zr, and patterns comparable to those of Arc-BABB-FAB system (e.g. Saunders and Tarney 1984).

The Ghalaylan basalts are graphically compared (Figure 11(a,b)) to Red Sea margin and Mariana intra-oceanic arc basalts, here chosen to represent the two major scenarios of (i) continental margin volcanic rocks and oceanic plateaus with OIB-signature erupted through continental lithosphere and (ii) intra-oceanic arc-basin system (see Pearce 2008 and references therein), respectively. In both Th/Yb vs. Nb/Yb and TiO_2/Yb vs. Nb/Yb proxy diagrams (Figure 11(a,b); after Pearce 2008), the Ghalaylan basalts show a distinctive OIB signature similar to Red Sea margin basalts (Hart *et al*. 1989; Barrat *et al*. 1990, 1993; Volker *et al*. 1997). Only unusual sample GL20 plots in the field of the Mariana arc (Pearce *et al*. 2005; Pearce 2008). In the Nb/La vs. εNd(t) diagram (Peate 1997; Anh *et al*. 2011), OIB-mantle origin is also confirmed by Nb/La ratios for the Ghalaylan basalts (Figure 11(c)), which also cluster around the Primitive Mantle (Nb/La: 1.04; McDonough and Sun 1995).

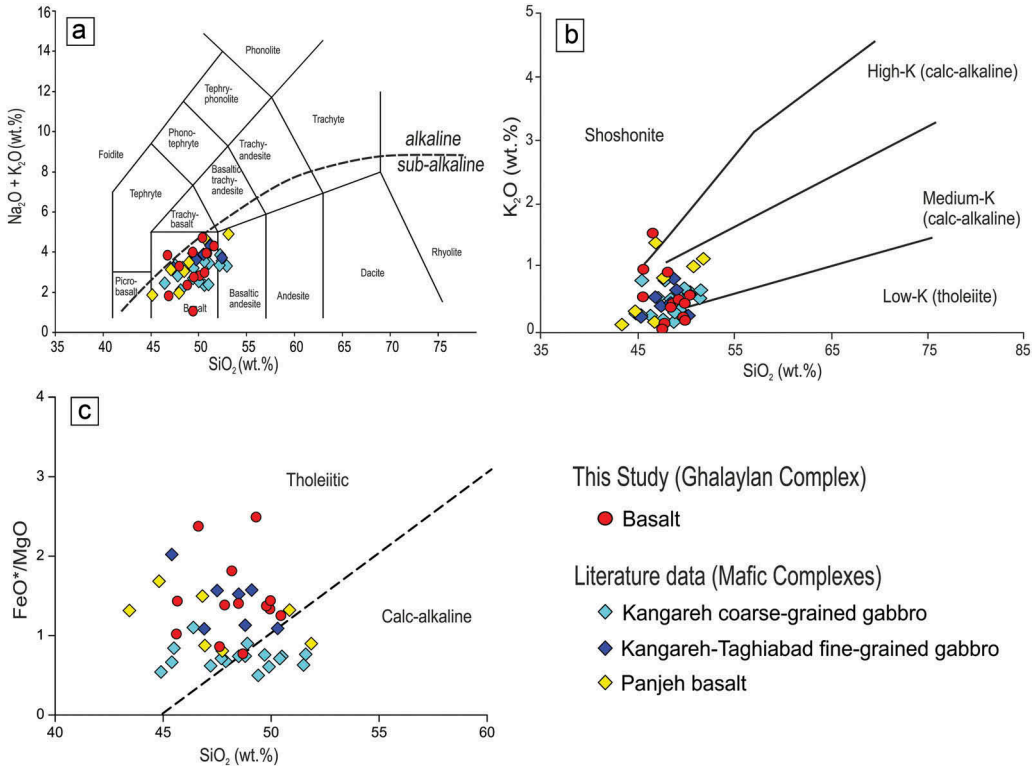

Figure 6. (a) Total alkalies – silica (TAS) chemical classification diagram (LeMaitre *et al*. 2002), showing that Ghalaylan mafic rocks plot in the basalt field. (c) In the K2O-SiO2 variation diagram most of the samples are plotted in the Low-K series. (c) In the FeOt/MgO vs SiO2 diagram (Miyashiro and Shido 1975; Dilek *et al*. 2008) Ghalaylan basalts present a clear tholeiitic signature.

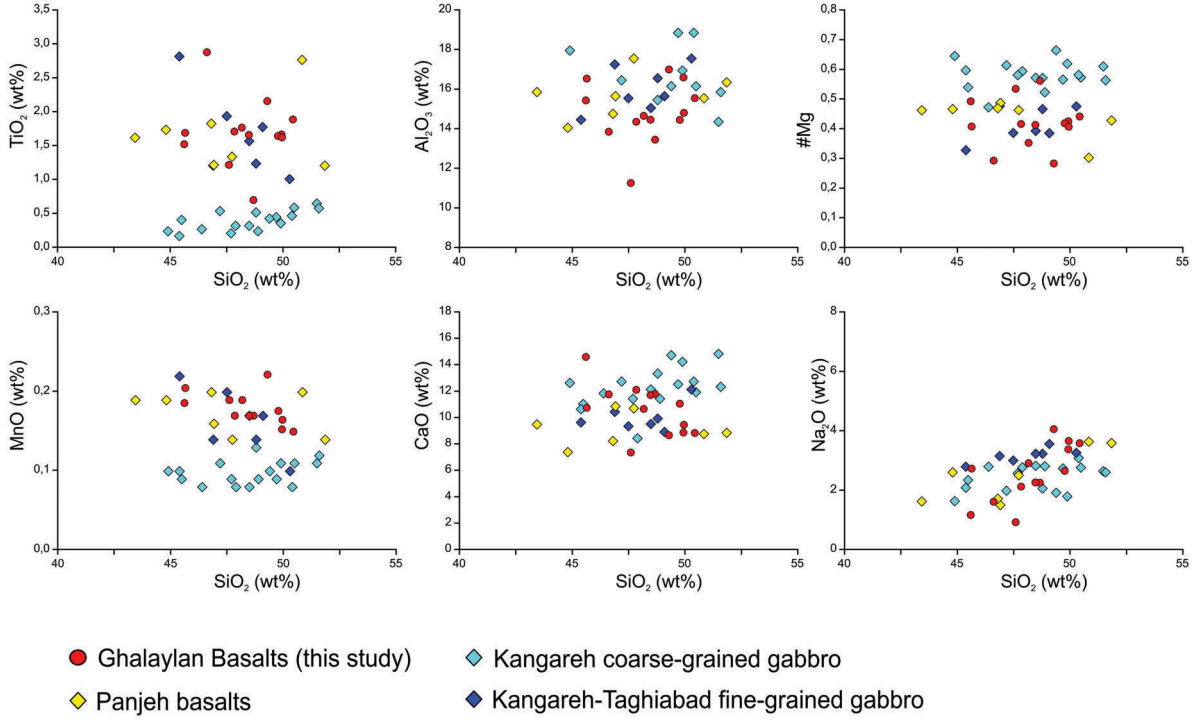

Figure 7. Harker diagrams for selected major oxides. SiO2 is the differentiation index and negatively correlates with MnO and CaO and positively correlates with Na2O, showing some minor magma differentiation for each group.

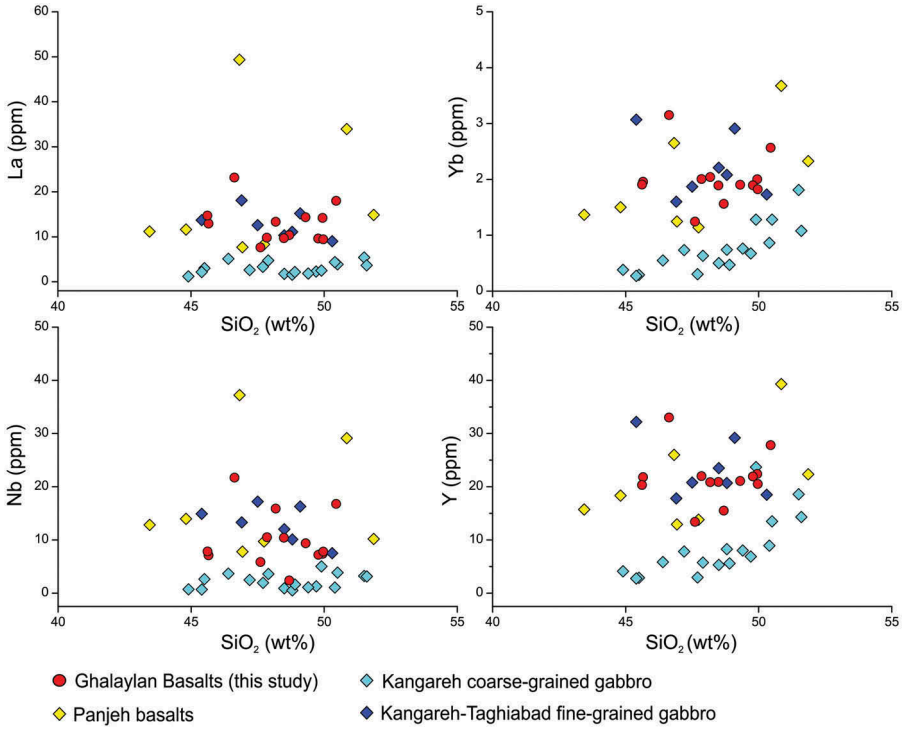

Figure 8. Both large ion lithophile elements (LILEs) and high field strength elements (HFSEs) show scattered distribution with no appreciable correlation.

7.2. Magma evolution

The Ghalayaban basalts range from near primitive (GL-26: 14.8 wt. % MgO, 620 ppm Ni, 1320 ppm Cr) to fractionated (GLZ4: 4.5 wt. % MgO, 22.1 ppm Ni, 33.5 ppm Cr). Because fractionation in the crust provides opportunities for crust and magma to interact, fractionated basalts are more likely to be contaminated by continental crust than are primitive basalts; correspondingly, primitive basalts are most likely to preserve chemical and isotopic information about their mantle source. Two samples (GL-21 and GL-26) contain >10 wt. % MgO, >130 ppm Ni, and >700 ppm Cr and are the least fractionated. These are geochemically and isotopically quite different, demonstrating strong heterogeneity in the mantle source region. This source heterogeneity is also revealed in trace element variations and Sr-Nd isotope ratios of all Ghalaylan metabasalts, which clearly define geochemically distinct groups that mostly reflect mantle source variability. In spite of strong heterogeneity in the mantle source, all Ghalaylan metabasalts show similar strongly-LREE-enriched patterns (Figure 9(a)). The plot of La/Yb versus Dy/Yb ratios (Figure 11(d)) can help distinguish between melting in the spinel and garnet stability fields (e.g., Thirlwall *et al.* 1994; Jung *et al.* 2012; Mayer *et al.* 2013). Modelling (Figure 11(d)) suggests that these melts were derived from ~5% melting of amphibole-spinel peridotite, but because of the similar effects of amphibole and garnet in fractionation HREE, a role for garnet peridotite cannot be excluded.

Important indications on the magma source can be gleaned from the Sr-Nd isotope ratios of the Ghalaylan basalts. These have $^{87}Sr/^{86}Sr(i)$ of 0.7039–0.7077 and εNd(t) ranging from +0.1 to +4.6, suggesting an OIB-like depleted mantle source, possibly affected by seawater alteration. Basaltic sample GL20 with εNd (t) = −7.8 and $^{87}Sr/^{86}Sr_{(145Ma)}$ = 0.7069 fall in the enriched mantle quadrant in the field of continental flood basalts of Hawkesworth *et al.* (1983) near the line indicating crust contamination (after Philpotts and Ague 2009). Nd model ages range widely, from 829 to 2080 Ma, with a mean of 1.1 Ga. This is somewhat older than expected for Cadomian SCLM, suggesting participation of some older mantle remnants.

In the Sr-Nd isotopic diagram (Figure 12), oceanic plateau and OIBs generally plot between the Depleted Mantle (DM) and the Chondritic Uniform Reservoir (CHUR) while the compositions of continental flood basalts generally plot in the field of Enriched Mantle (negative εNd(t), and enriched $^{87}Sr/^{86}Sr(i)$), indicating interaction/contamination with lithospheric mantle and/or continental crust (Campbell and Griffiths 1990; Ellam and Cox 1991; Saunders *et al.* 1992; Chung and Jahn 1995; Ernst and Buchan 2003; Qin *et al.* 2011). On

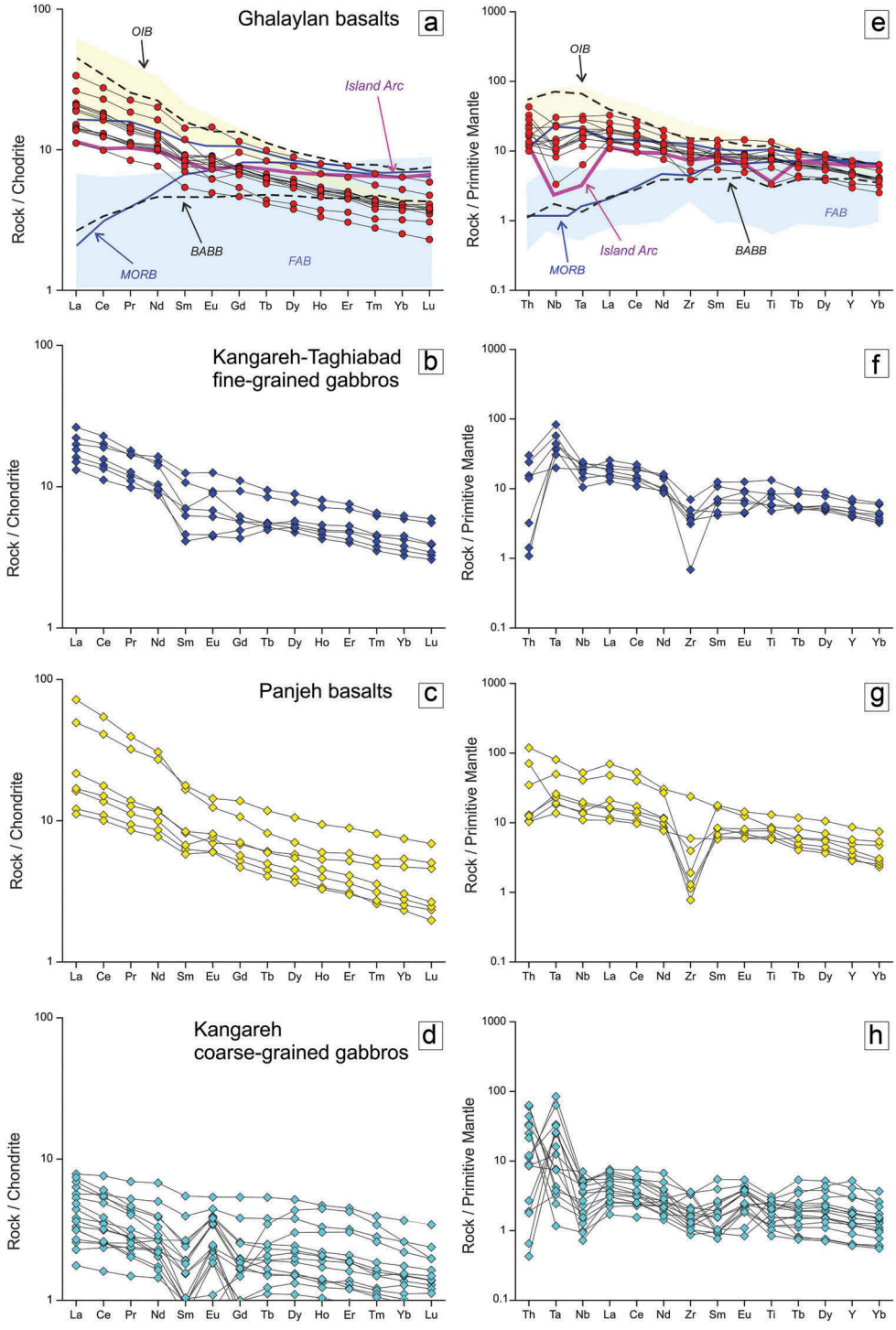

Figure 9. Chondrite-normalized REE diagrams (after Sun and McDonough 1989) (a–d) for Ghalaylan, Panjeh, Kangareh and Taghiabad mafic rocks and Primitive mantle normalized trace element diagrams (e–h). Petrological group and references: BABB, back arc basalts (Pearce *et al*. 2005; Buchs *et al*. 2013); FAB, forearc basalts (Reagan *et al*. 2010; Ishizuka *et al*. 2011); MORB, mid-ocean ridge basalts (Jenner and O'Neill 2012); OIB, ocean island basalts (Willbold and Stracke 2006; Buchs *et al*. 2013). Island arc basalts after Buchs *et al*. (2013).

the εNd(t) vs. $^{87}Sr/^{86}Sr(i)$ diagram (Figure 12) the Ghalaylan samples show OIB-like Sr-Nd isotopic signatures comparable to those of Afar and Emeishan continental flood basalts. Ghalaylan GL20 basalt sample with (i) high TiO_2 (1.9 wt%), Yb (2.57 ppm), Nb (16.8 ppm), Y (27.8 ppm) values, (ii) highest SiO_2 (50.5 wt%) and Th (3.62 ppm) contents, and (iii) negative εNd(t) (−7.8) value show clear affinities with both Tarim and

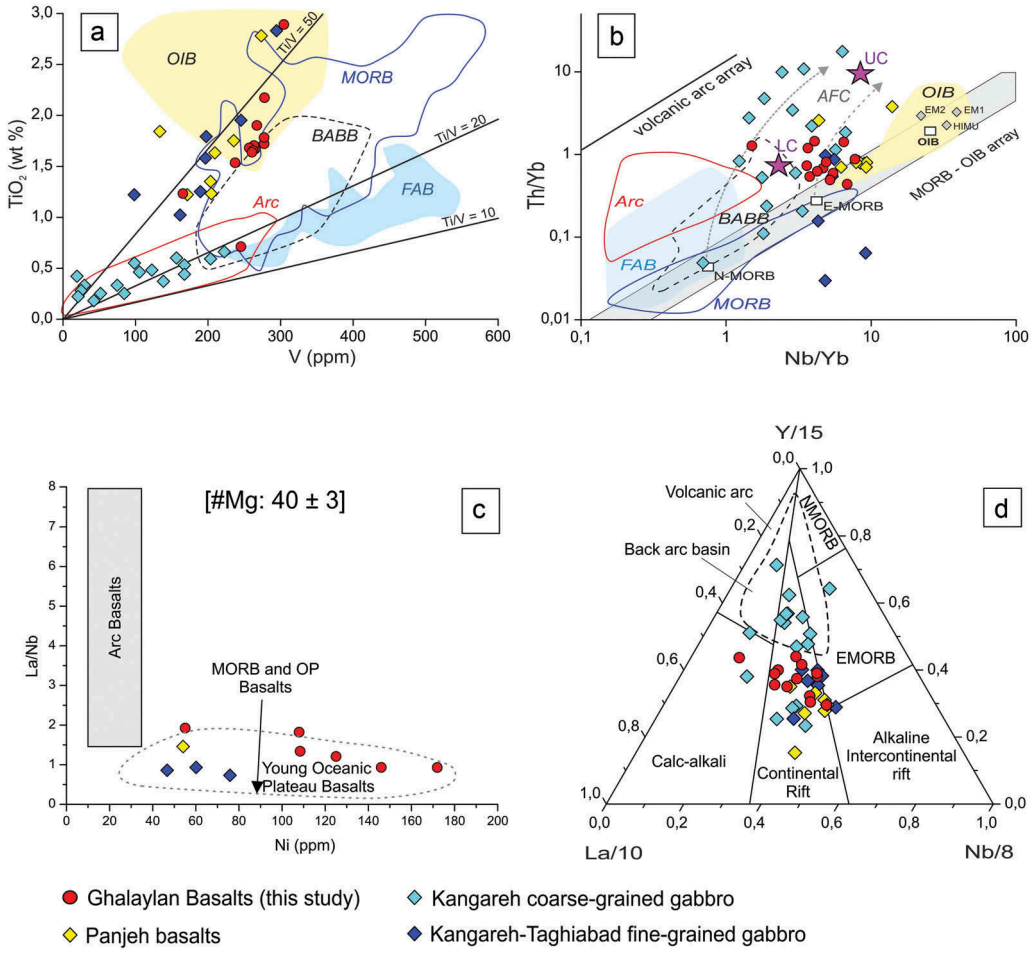

Figure 10. (a) In TiO2 vs. V diagram (Shervais 1982; Reagan *et al*. 2010), the Ghalaylan samples, with Ti/V ranging 37–57, show OIB-like signature. Arc-like signature is recognized only for sample GL21 with TiO2 < 1.0 wt. % and Ti/V ratio of 17. (b) In Th/Yb vs Nb/Yb diagram (Pearce 2008), the Ghalaylan basalts plot along and above the MORB-OIB array, falling near E-MORB. (c) The La/Nb ratios and Ni content for Mg#40 (= Ni40; Condie 1999). Samples with Mg# = 40 ± 3 were plotted. The calculation of the Ni40 for the basaltic rocks in the Ghalaylan area shows that these rocks mainly have high Ni40 (40–180 ppm) and low La/Nb, clearly distinguishing them from arc basalts. (d) La-Y-Nb (Cabanis and Lecolle 1989) diagram, which classifies the Ghalaylan mafic rocks as rift basalt, different from back arc setting. The back arc basin basalts field is from Shinjo *et al*. (1999).

Table 3. Whole rocks isotope ratios of Ghalylan complex.

Sample	Rock	$^{87}Rb/^{86}Sr$	$^{87}Sr/^{86}Sr(p)$	±1SE	$^{87}Sr/^{86}Sr(i)$	$^{147}Sm/^{144}Nd$	$^{143}Nd/^{144}Nd(p)$	±1SE	$^{143}Nd/^{144}Nd(i)$	$\varepsilon^{Nd}(t)$	T_{DM}
GL20	Basalt	0.140	0.707273	0.000041	0.7070	0.143	0.512188	0.000011	0.51205	−7.8	2080
GL21	Basalt	0.0711	0.704068	0.000052	0.7039	0.141	0.512742	0.000004	0.51261	3.1	859
GL22	Basalt	0.0688	0.704948	0.000055	0.7048	0.154	0.512807	0.000004	0.51266	4.1	871
GL23	Basalt	0.0153	0.704677	0.000172	0.7046	0.157	0.512836	0.000004	0.51268	4.6	845
GL24	Basalt	0.632	0.709026	0.000061	0.7077	0.141	0.512591	0.000004	0.51246	0.1	1170
GL25	Basalt	0.198	0.706264	0.000025	0.7058	0.136	0.512693	0.000004	0.51256	2.2	892
GL26	Basalt	0.267	0.707835	0.000065	0.7073	0.140	0.512749	0.000004	0.51261	3.2	829
GLZ1	Basalt	0.204	0.706142	0.000007	0.7057						
GLZ2	Basalt	0.095	0.706191	0.000006	0.7060						
GLZ4	Basalt	0.122	0.706716	0.000006	0.7065						
GLZ6	Basalt	0.104	0.707516	0.000006	0.7073						
GLZ7	Basalt	0.038	0.705415	0.000006	0.7053						
GLZ8	Basalt	0.033	0.705196	0.000006	0.7051						

The natural Sr and Nd isotope ratios were normalized based on $^{146}Nd/^{144}Nd = 0.7219$ and $^{86}Sr/^{88}Sr = 0.1194$. Averages and 1SD for isotope ratio standards, NIST-SRM987 and JNdi-1, were $^{87}Sr/^{86}Sr = 0.710244 \pm 0.000009$ (n = 11) and $^{143}Nd/^{144}Nd = 0.512113 \pm 0.00006$ (n = 9). The CHUR (Chondritic Uniform Reservoir) values, $^{147}Sm/^{144}Nd = 0.1967$ and $^{143}Nd/^{144}Nd = 0.512638$, were used to calculate the ε0(DePaolo and Wasserburg 1976). $T_{DM} = 1/\lambda \ln [((^{143}Nd/^{144}Nd)_{sample}-0.51315)/((^{147}Sm/^{144}Nd)_{sample}-0.2137)+1]$.

p = present, i = initial, SE = standard error.

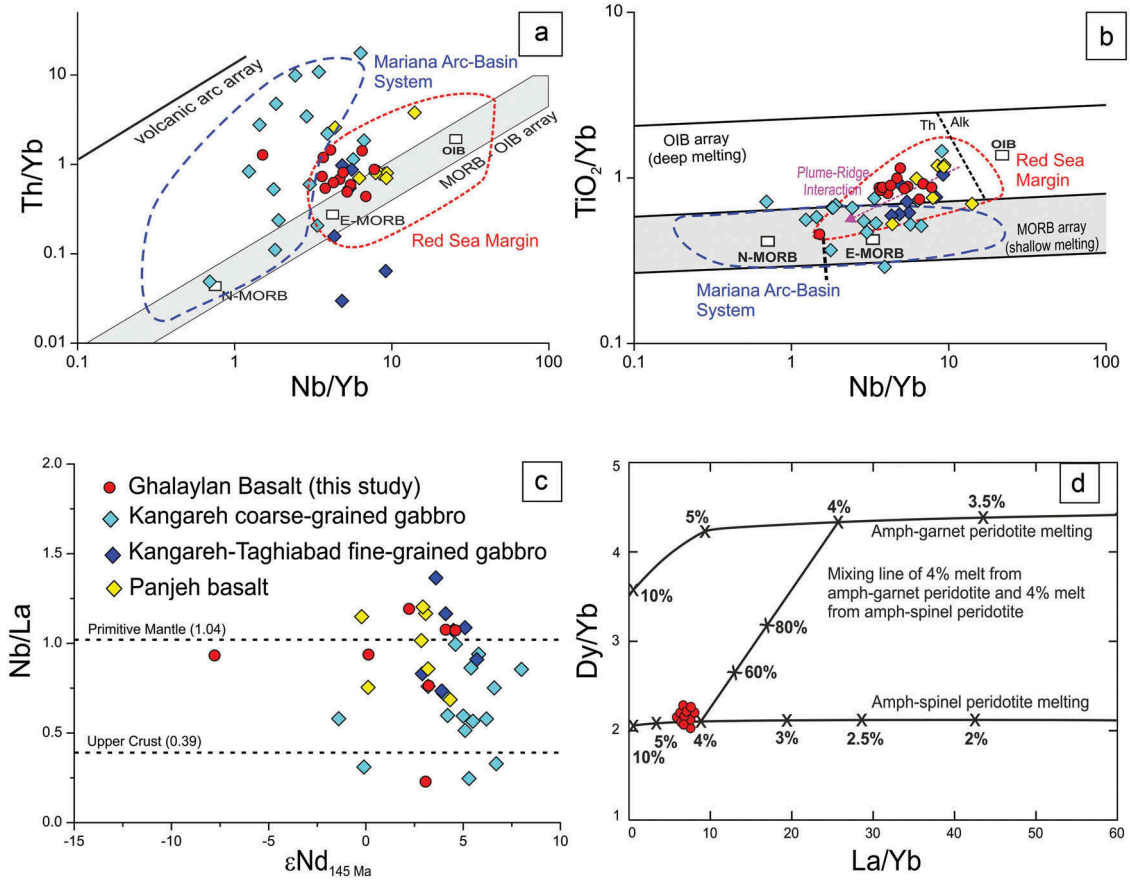

Figure 11. (a, b) In both Th/Yb vs. Nb/Yb and TiO2/Yb vs. Nb/Yb proxy diagrams Ghalaylan basalts show a distinct OIB signature and fall mainly in the field of Red Sea margin basalts (Hart *et al*. 1989; Barrat *et al*. 1990, 1993; Volker *et al*. 1997; Pearce 2008). Only sample GL21 in both diagrams is different, plotting in the field of Mariana arc lavas (Pearce *et al*. 2005; Pearce 2008). (c) Nb/La vs. ? Nd(t) diagram. An OIB-mantle origin is also confirmed by Nb/La ratios (Peate 1997; Anh *et al*. 2011) for the Ghalaylan basalts showing Nb/La ratio mean value close to that of Primitive Mantle melts (Nb/La: 1.04; McDonough and Sun 1995). (d) Plot of La/Yb versus Dy/Yb ratios for distinguishing between partial melting of peridotite in the spinel and garnet stability fields (e.g., Thirlwall *et al*. 1994; Jung *et al*. 2012; Mayer *et al*. 2013). The Ghalaylan basalts formed by 5–8% melt from spinel-facies mantle.

Emeishan Large Igneous Plateaus (LIPs). Unusual sample GL21 again is distinctive with the lowest $^{87}Sr/^{86}Sr(i)$ (~0.7039) falling inside the restricted field of IBM intra-oceanic arc basalts.

These results indicate that the source mantle was heterogeneous but mostly was not metasomatized by hydrous fluids or sediment melts from a Jurassic subducted slab. Given that the crust is largely Cadomian in age, it seems likely that partial melting of subcontinental lithospheric mantle of Cadomian age contributed to forming Ghalaylan basaltic magmas. Some of this mantle may have been affected by Cadomian subduction to produce rare arc-like melts represented by GL21.

7.3. Implications for resolving the Jurassic SaSZ controversy

Formation as a magmatic arc (e.g. Tatsumi 2005; Pichavant and Macdonald 2007; Zhang *et al*. 2011) is the dominant interpretation for Jurassic SaSZ igneous activity (e.g., Berberian and Berberian 1981; Berberian *et al*. 1982; Mohajjel *et al*. 2003; Ghasemi and Talbot 2006; Davoudian *et al*. 2008). Recent studies (Azizi *et al*. 2015a, 2018) challenge this interpretation for the northern-central SaSZ, and in particular for the Songhor-Ghorveh area.

Based on (i) chemical composition of Ghalaylan basalts and (ii) their clear OIB-signature, we explore the possibility that they are not the result of convergent margin magmatism.

Considering the (i) geochemical evidence and (ii) the Afar-like Sr-Nd isotopic signature (Figure 12) highlighted in this work, we propose that Ghalaylan basalts are the product of OIB-like magmatism associated with continental rifting and/or mantle plume beneath the SaSZ in Upper Jurassic time (ca. 160–144 Ma.).

It is worth noting that a similar scenario of continental rifting associated with OIB-like magmatism due to

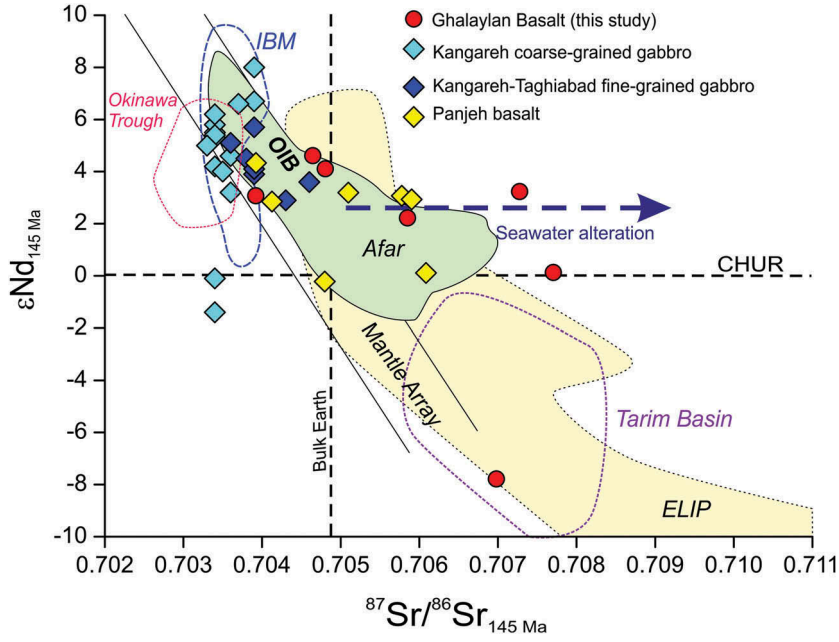

Figure 12. Comparison of ?Nd(t) vs. 87Sr/86Sr(i) between the Ghalaylan basalts and (i) OIB-melt, (ii) LIP and continental flood basalts and (iii) Intra-oceanic arc-basin magmatism. Basalts from Afar depression (Hart *et al*. 1989; Kampunzu and Mohr 1991; Vidal *et al*. 1991; Deniel *et al*. 1994; Rogers 2006) are selected as representative of OIB-melts from plume activity under continental crust since their unambiguous signature of mantle plume (Rogers 2006 and references therein). Fields of the Emeishan large igneous province (ELIP) in SW China (Chung and Jahn 1995; Xu *et al*. 2001, 2004; Ali *et al*. 2005; Anh *et al*. 2011; Song *et al*. 2011) and Tarim Basin in NW China (Zhang *et al*. 2003; Xia *et al*. 2006; Yang *et al*. 2007; Li *et al*. 2008; Chen *et al*. 2009; Zhou *et al*. 2009; Tian *et al*. 2010; Qin *et al*. 2011) are shown. Izu-Bonin-Mariana (IBM) arc-lavas (Stern *et al*. 2003; Reagan *et al*. 2010; Ishizuka *et al*. 2011) are chosen as representing an intra-oceanic arc-basin system. The Ghalaylan samples show OIB-like Sr-Nd isotopic signature comparable to those of Afar plume and Emeishan Traps (ELIP). To note that Ghalaylan GL20 basalt sample characterized by (i) higher TiO2 (1.9 wt.%), Yb (2.57 ppm), Nb (16.8 ppm), Y (27.8 ppm) values, (ii) highest SiO2 (50.5 wt.%) and Th (3.62 ppm) contents, (iii) relatively low #Mg (44) and (iv) negative ?Nd(t) (−7.8) value show clear affinities with both Tarim and Emeishan LIPs basalts. Ghalaylan GL21 basalt shows a different distinctive signature with strong depletion in 87Sr/86Sr(i) ratio and fall inside the narrow field of IBM representing intra-oceanic arc-basin system.

mantle plumes activity in Late Jurassic-Early Cretaceous is reported for the Silesian basin (western Carpathians, Eurasian plate) (Golonka *et al*. 2006 and references therein). In their work on the circum-Carpathian region, Golonka *et al*. (2006) integrated position of Upper Jurassic magmatics (Lucin´ska-Anczkiewicz *et al*. 2000; Golonka *et al*. 2006) and Early Cretaceous volcanics (Lashkevitsch *et al*. 1995, Lewandowski et al., 2003) with Mesozoic plate tectonic models in a Pangea framework and identified a correspondence between Jurassic-Cretaceous coordinates of Silesian basin magmatism and current position of both western Turkey and Levantine (e.g. Dead Sea) hot spots. In their plate-tectonic evolution model, Golonka *et al*. (2006) suggest therefore that the Silesian rifting and the OIB-magmatism at Late Jurassic-Early Cretaceous was a possible evidence of western Carpathian domain passing over the head of the Levantine plume.

Considering the OIB-like signature at 155–158 Ma of Kangareh-Taghiabad fine-grained gabbros (Azizi *et al*. 2018) intruding the Triassic to Middle Jurassic marine sedimentary sequence (Oxfordian-Kimmeridgian; Azizi *et al*. 2015a), we hypothesize that rifting began by Middle Jurassic – Upper Jurassic time and we think that further useful constraints on the evolution of this continental rift might be obtained, in future studies, by reconstructing the subsidence history of Jurassic sediments.

Finally, the reinterpretation of Jurassic igneous activity in the SaSZ as rift- and/or plume-related, opens new questions on initiation and timing of the Neotethys subduction beneath the SW margin of Asia. If Jurassic SaSZ magmatism does not reflect an arc setting, there is no reason to further invoke an active subduction zone at that time. This should be taken into account in future efforts to reconstruct the tectonic evolution of the region in Mesozoic time.

8. Conclusions

The Ghalaylan basaltic complex represents a key for deciphering the Late Jurassic tectono-magmatic

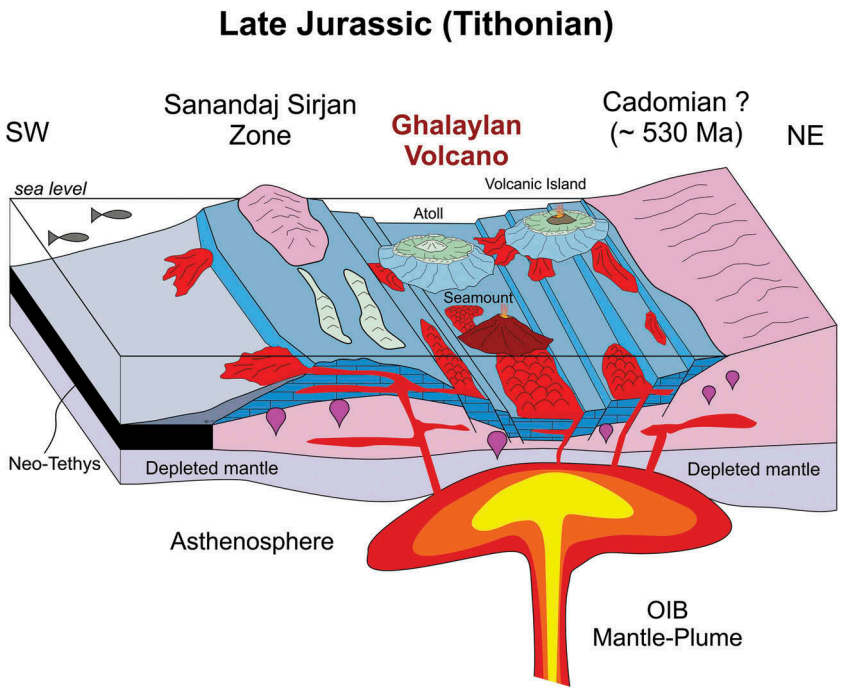

Figure 13. Schematic conceptual model showing the generation of the Ghalaylan basaltic rocks and probably as a seamount in an extensional basin and its relation to the OIB type plume.

evolution of the Songhor-Ghorveh area in the northern Sanandaj-Sirjan zone. Significant outcomes of our study include:

- Ghalaylan basaltic lava flows and pillows are the evidence of a submarine volcano active at ca. 144 Ma (as determined by zircon U-Pb dating). Whole rock geochemistry is comparable to the neighbourhood Late Jurassic basaltic complexes of Panjeh and Kangareh-Taghiabad;
- Ghalaylan submarine volcano formed on thinned Cadomian continental crust with Triassic to Middle-Late Jurassic marine sediments, a tectonic setting consistent with continental rifting;
- Ghalaylan basalt whole-rock and Sr-Nd isotope geochemistry show OIB-like compositions compatible with ~ 5% melting of heterogeneous subcontinental lithosphere and/or plume mantle. Only minor evidence of interaction/assimilation of continental crust are recognized;
- Trace element geochemistry and Sr-Nd isotope compositions of Ghalaylan basalts overlap those of Afar, Emeishan LIP and Tarim Basin mafic rocks, representative of OIB magmatism in continental rifting due to the activity of mantle-plumes.

To conclude, results obtained in this study, and comparison with existing data for neighbourhood Panjeh, and Kangareh-Taghiabad mafic complexes of Late Jurassic age answer the 'Jurassic SaSZ controversy' in favour of a magmatic continental rift.

Acknowledgments

We thank P. Cipollari for discussion and advice. This research was supported by the University of Kurdistan for fieldwork and Nagoya University and JSPS KAKENHI Grant (Nos. 25303029, 17H01671) and join research program of the Institute for Space – Earth Environmental Research (ISEE), Nagoya University. H. Azizi would like to thank both University of Kurdistan and Nagoya University for their support during his sabbatical periods in 2017-18. This is UTD Geosciences contribution number 13XX. This version much benefits from comments by the associate editor, Hadi Shafaii Moghadm, anonymous reviewers and Reza Maghdour-Mashhour.

Disclosure statement

No potential conflict of interest was reported by the authors.

Funding

Japan Society for the Promotion of Sciences (JSPS) KAKENHI Grant [Nos. 25303029, 17H01671] and join research program of the Institute for Space – Earth Environmental Research (ISEE), Nagoya University.

ORCID

Hossein Azizi http://orcid.org/0000-0001-5686-4340

References

Ahmadi-Khalaji, A., Tahmasbi, Z., Rahmani, S., and Basiri, S., 2015, The geochemical and tectonic characteristics of the volcanic rocks in the east of Nahavand area (Sanandaj-Sirjan zone): Petrology, v. 23, p. 1–26. (in Persian).

Ahmadi-Khalaji, A.A., Esmaeily, D., Valizadeh, M.V., and Rahimpour-Bonab, H., 2007, Petrology and geochemistry of the granitoid complex of Boroujerd, Sanandaj-Sirjan Zone, Western Iran: Journal of Asian Earth Sciences, v. 29, p. 859–877. doi:10.1016/j.jseaes.2006.06.005

Ahmadipour, H., Sabzehei, M., Emami, M., Whitechurch, H., and Rastad, E., 2003, Soghan complex as an evidence for paleo spreading center and mantle diapirism in Sanandaj-Sirjan zone (south-east Iran): Islamic Azad University: Mashhad Branch, v. 14, p. 157–172.

Alavi, M., 1994, Tectonics of the Zagros orogenic belt of Iran: New data and interpretations: Tectonophysics, v. 229, p. 211–238. doi:10.1016/0040-1951(94)90030-2

Ali, J.R., Thompson, G.M., Zhou, M.F., and Song, X., 2005, Emeishan large igneous province, SW China: Lithos, v. 79, p. 475–489. doi:10.1016/j.lithos.2004.09.013

Aliani, F., Maanijou, M., Sabouri, Z., and Sepahi, A.A., 2012, Petrology, geochemistry and geotectonic environment of the Alvand Intrusive Complex, Hamedan, Iran: Chemie der Erde-Geochemistry, v. 72, p. 363–383. doi:10.1016/j.chemer.2012.05.001

Anh, T.V., Pang, K.N., Chung, S.L., Lin, H.M., Hoa, T.T., Anh, T.T., and Yang, H.J., 2011, The Song Da magmatic suite revisited: A petrologic, geochemical and Sr–Nd isotopic study on picrites, flood basalts and silicic volcanic rocks: Journal of Asian Earth Sciences, v. 42, p. 1341–1355. doi:10.1016/j.jseaes.2011.07.020

Arndt, N.T., and Jenner, G.A., 1986, Crustally contaminated komatiites and basalts from Kambalda, Western Australia: Chemical Geology, v. 56, p. 229–255. doi:10.1016/0009-2541(86)90006-9

Arvin, M., Pan, Y., Dargahi, S., Malekizadeh, A., and Babaei, A., 2007, Petrochemistry of the Siah-Kuh granitoid stock southwest of Kerman, Iran: Implications for initiation of Neotethys subduction: Journal of Asian Earth Sciences, v. 30, p. 474–489. doi:10.1016/j.jseaes.2007.01.001

Ayalew, D., Jung, S., Romer, R.L., Kersten, F., Pfänder, J.A., and Garbe-Schönberg, D., 2016, Petrogenesis and origin of modern Ethiopian rift basalts: Constraints from isotope and trace element geochemistry: Lithos, v. 258, p. 1–14. doi:10.1016/j.lithos.2016.04.001

Azizi, H., and Asahara, Y., 2013, Juvenile granite in the Sanandaj–Sirjan Zone, NW Iran: Late Jurassic–Early Cretaceous arc–Continent collision: International Geology Review, v. 55, p. 1523–1540. doi:10.1080/00206814.2013.782959

Azizi, H., Asahara, Y., Mehrabi, B., and Chung, S.L., 2011, Geochronological and geochemical constraints on the petrogenesis of high-K granite from the Suffi abad area, Sanandaj-Sirjan Zone, NW Iran: Chemie der Erde-Geochemistry, v. 71, p. 363–376. doi:10.1016/j.chemer.2011.06.005

Azizi, H., Beiranvand, M.Z., and Asahara, Y., 2015b, Zircon U–Pb ages and petrogenesis of a tonalite–Trondhjemite–Granodiorite (TTG) complex in the Northern Sanandaj–Sirjan Zone, Northwest Iran: Evidence for Late Jurassic arc–Continent collision: Lithos, v. 216–217, p. 178–195. doi:10.1016/j.lithos.2014.11.012

Azizi, H., Lucci, F., Stern, R.J., Hasannejad, S., and Asahara, Y., 2018, The Late Jurassic Panjeh submarine volcano in the northern Sanandaj-Sirjan Zone, northwest Iran: Mantle plume or active margin?: Lithos, v. 308, p. 364–380. doi:10.1016/j.lithos.2018.03.019

Azizi, H., Mohammadi, K., Asahara, Y., Tsuboi, M., Daneshvar, N., and Mehrabi, B., 2016, Strongly peraluminous leucogranite (Ebrahim-Attar granite) as evidence for extensional tectonic regime in the Cretaceous, Sanandaj Sirjan zone, Northwest Iran: Chemie der Erde-Geochemistry, v. 76, p. 529–541. doi:10.1016/j.chemer.2016.08.006

Azizi, H., Najari, M., Asahara, Y., Catlos, E.J., Shimizu, M., and Yamamoto, K., 2015a, U–Pb zircon ages and geochemistry of Kangareh and Taghiabad mafic bodies in northern Sanandaj–Sirjan Zone, Iran: Evidence for intra-oceanic arc and back-arc tectonic regime in Late Jurassic: Tectonophysics, v. 47-64, p. 660. doi:10.1016/j.tecto.2015.08.008

Badr, A., Davoudian, A.R., Shabanian, N., Azizi, H., Asahara, Y., Neubauer, F., Dong, Y., and Yamamoto, K., 2018, A-and I-type metagranites from the North Shahrekord metamorphic complex, Iran: Evidence for early Paleozoic post-collisional magmatism: Lithos, v. 300, p. 86–104. doi:10.1016/j.lithos.2017.12.008

Baharifar, A., Moinevaziri, H., Bellon, H., and Piqué, A., 2004, The crystalline complexes of Hamadan (Sanandaj–Sirjan zone, western Iran): Metasedimentary Mesozoic sequences affected by Late Cretaceous tectono-metamorphic and plutonic events: Comptes Rendus Geoscience, v. 336, p. 1443–1452. doi:10.1016/j.crte.2004.09.014

Barrat, J.A., Jahn, B.M., Fourcade, S., and Joron, J.L., 1993, Magma genesis in an ongoing rifting zone: The Tadjoura Gulf (Afar area): Geochimica et cosmochimica acta, v. 57, p. 2291–2302. doi:10.1016/0016-7037(93)90570-M

Barrat, J.A., Jahn, B.M., Joron, J.L., Auvray, B., and Hamdi, H., 1990, Mantle heterogeneity in northeastern Africa: Evidence from Nd isotopic compositions and hygromagmaphile element geochemistry of basaltic rocks from the Gulf of Tadjoura and southern Red Sea regions: Earth and Planetary Science Letters, v. 101, p. 233–247. doi:10.1016/0012-821X(90)90156-R

Bayati, M., Esmaeili, D., Maghdour-Mashhour, R., Li, X.H., and Stern, R.J., 2017, Geochemistry and petrogenesis of Kolah Ghazi granitoids of Iran: Insights into the Jurassic Sanandaj-Sirjan magmatic arc: Chemie der Erde-Geochemistry, v. 77, p. 281–302. doi:10.1016/j.chemer.2017.02.003

Berberian, F., and Berberian, M., 1981, Tectono-plutonic episodes in Iran: Zagros Hindu Kush Himalaya geodynamic evolution, edited by H. K. Gupta and F. M. Delany: American Geophysical Union, v. 3, p. 33–69. doi:10.1029/GD003p0005

Berberian, F., Muir, I.D., Pankhurst, R.J., and Berberian, M., 1982, Late Cretaceous and early Miocene Andean-type plutonic activity in northern Makran and Central Iran: Journal of the Geological Society, v. 139, p. 605–614. doi:10.1144/gsjgs.139.5.0605

Buchs, D.M., Bagheri, S., Martin, L., Hermann, J., and Arculus, R., 2013, Paleozoic to Triassic ocean opening and closure preserved in Central Iran: Constraints from the geochemistry of meta-igneous rocks of the Anarak area: Lithos, v. 172, p. 267–287. doi:10.1016/j.lithos.2013.02.009

Cabanis, B., and Lecolle, M., 1989, Le diagramme La/10-Y/15-Nb/8 un outil pour la discrimination des series volcaniques et la mise en evidence des processus de mélange et/ou de contamination crustale: CRAS Paris, v. 309, p. 2023–2029.

Campbell, I.H., and Griffiths, R.W., 1990, Implications of mantle plume structure for the evolution of flood basalts: Earth and Planetary Science Letters, v. 99, p. 79–93. doi:10.1016/0012-821X(90)90072-6

Chen, H.L., Yang, S.F., Li, Z.L., Yu, X., Luo, J.C., He, G.Y., Lin, X.B., and Wang, Q.H., 2009, Spatial and temporal characteristics of Permian large igneous province in Tarim Basin: Xinjiang Petroleum Geology, v. 30, p. 179–182. doi:10.1016/0012-821X(90)90072-6

Chiu, H.Y., Chung, S.L., Zarrinkoub, M.H., Mohammadi, S.S., Khatib, M.M., and Iizuka, Y., 2013, Zircon U–Pb age constraints from Iran on the magmatic evolution related to Neotethyan subduction and Zagros orogeny: Lithos, v. 162, p. 70–87. doi:10.1016/j.lithos.2013.01.006

Chung, S.L., and Jahn, B.M., 1995, Plume-lithosphere interaction in generation of the Emeishan flood basalts at the Permian-Triassic boundary: Geology, v. 23, p. 889–892. doi:10.1130/0091-7613(1995)023%3C0889: PLIIGO%3E2.3.CO

Condie, K.C., 1999, Mafic crustal xenoliths and the origin of the lower continental crust: Lithos, v. 46, p. 95–101. doi:10.1016/S0024-4937(98)00056-5

Davoudian, A.R., Genser, J., Dachs, E., and Shabanian, N., 2008, Petrology of eclogites from north of Shahrekord, Sanandaj-Sirjan Zone, Iran: Mineralogy and Petrology, v. 92, p. 393–413. doi:10.1007/s00710-007-0204-6

Deevsalar, R., Ghorbani, M.R., Ghaderi, M., Ahmadian, J., Murata, M., Ozawa, H., and Shinjo, R., 2014, Geochemistry and petrogenesis of arc-related to intraplate mafic magmatism from the Malayer-Boroujerd plutonic complex, northern Sanandaj-Sirjan magmatic zone, Iran: Neues Jahrbuch für Geologie und Paläontologie-Abhandlungen, v. 274, p. 81–120. doi:10.1127/njgpa/2014/0435

Deevsalar, R., Shinjo, R., Liégeois, J.P., Valizadeh, M.V., Ahmadian, J., Yeganehfar, H., Murata, M., and Neill, I., 2017, Subduction-related mafic to felsic magmatism in the Malayer–Boroujerd plutonic complex, western Iran: Swiss Journal of Geosciences, v. 111, p. 1–25. doi:10.1007/s00015-017-0287-y

Deniel, C., Vidal, P., Coulon, C., Vellutini, P.J., and Piguet, P., 1994, Temporal evolution of mantle sources during continental rifting: The volcanism of Djibouti (Afar): Journal of Geophysical Research Solid Earth, v. 99, p. 2853–2869. doi:10.1029/93JB02576

DePaolo, D.J., and Wasserburg, G.J., 1976, Nd isotopic variations and petrogenetic models: Geophysical Research Letters, v. 3, p. 249–252. doi:10.1029/GL003i005p00249

Dilek, Y., and Furnes, H., 2014, Ophiolites and their origins: Elements, v. 10, p. 93–100. doi:10.2113/gselements.10.2.93

Dilek, Y., Furnes, H., and Shallo, M., 2008, Geochemistry of the Jurassic Mirdita Ophiolite (Albania) and the MORB to SSZ evolution of a marginal basin oceanic crust: Lithos, v. 100, p. 174–209. doi:10.1016/j.lithos.2007.06.026

Eftekharnejad, J., 1981, Tectonic division of Iran with respect to sedimentary basins: Journal of Iranian Petroleum Society, v. 82, p. 19–28. (*(in Persian)*).

Eggins, S.M., Kinsley, L.P.J., and Shelley, J.M.M., 1998, Deposition and elemental fractionation processes during atmospheric pressure laser sampling for analysis by ICPMS: Applied Surface Science, v. 127–129, p. 278–286. doi:10.1016/S0169-4332(97)00643-0

Ellam, R.M., and Cox, K.G., 1991, An interpretation of Karoo picrite basalts in terms of interaction between asthenospheric magmas and the mantle lithosphere: Earth and Planetary Science Letters, v. 105, p. 330–342. doi:10.1016/0012-821X(91)90141-4

Ernst, R.E., and Buchan, K.L., 2003, Recognizing mantle plumes in the geological record: Annual Review of Earth and Planetary Sciences, v. 31, p. 469–523. doi:10.1146/annurev.earth.31.100901.145500

Esmaeily, D., Nédélec, A., Valizadeh, M.V., Moore, F., and Cotten, J., 2005, Petrology of the Jurassic Shah-Kuh granite (eastern Iran), with reference to tin mineralization: Journal of Asian Earth Sciences, v. 25, p. 961–980. doi:10.1016/j.jseaes.2004.09.003

Fazlnia, A., Schenk, V., van der Straaten, F., and Mirmohammadi, M., 2009, Petrology, geochemistry, and geochronology of trondhjemites from the Qori Complex, Neyriz, Iran: Lithos, v. 112, p. 413–433. doi:10.1016/j.lithos.2009.03.047

Gao, J.F., and Zhou, M.F., 2013, Generation and evolution of siliceous high magnesium basaltic magmas in the formation of the Permian Huangshandong intrusion (Xinjiang, NW China): Lithos, v. 162, p. 128–139. doi:10.1016/j.lithos.2013.01.002

Ghasemi, A., and Talbot, C.J., 2006, A new tectonic scenario for the Sanandaj–Sirjan Zone (Iran): Journal of Asian Earth Sciences, v. 26, p. 683–693. doi:10.1016/j.jseaes.2005.01.003

Golonka, J., 2004, Plate tectonic evolution of the southern margin of Eurasian the Mesozoic and Cenozoic: Tectonophysics, v. 381, p. 235–273. doi:10.1016/j.tecto.2002.06.004

Golonka, J., Gahagan, L., Krobicki, M., Marko, F., and Oszczypko, N., 2006, Plate-tectonic evolution and paleogeography of the circum-Carpathian region: AAPG Special Volumes,V, v. 84, p. 11–46. doi:10.1306/985606M843066

Günther, D., and Heinrich, C.A., 1999, Enhanced sensitivity in laser ablation–ICP mass spectrometry using helium–Argon mixtures as aerosol carrier: Journal of Analytical Atomic Spectrometry, v. 14, p. 1363–1368. doi:10.1039/A901648A

Hart, W.K., Woldegabriel, G., Walter, R.C., and Mertzman, S.A., 1989, Basaltic volcanism in Ethiopia: Constraints on continental rifting and mantle interactions: Journal of Geophysical Research Solid Earth, v. 94, p. 7731–7748. doi:10.1029/JB094iB06p07731

Hassanzadeh, J., Stockli, D.F., Horton, B.K., Axen, G.J., Stockli, L.D., Grove, M., Schmitt, A.K., and Walker, J.D., 2008, U-Pb zircon geochronology of late Neoproterozoic–Early Cambrian granitoids in Iran: Implications for paleogeography, magmatism and exhumation history of Iranian basement: Tectonophysics, v. 451, p. 71–96. doi:10.1016/j.tecto.2007.11.062

Hawkesworth, C.J., Erlank, A.J., Marsh, J.S., Menzies, M.A., and Van Calsteren, P., In Continental basalts and mantle xenoliths

(eds. C. J. Hawkesworth and M. J. Norry) pp. 111–138. Shiva Publ. Ltd., Cheshire.

Honarmand, M., Li, X.H., Nabatian, G., and Neubauer, F., 2017, In-situ zircon U-Pb age and Hf-O isotopic constraints on the origin of the Hasan-Robat A-type granite from Sanandaj–Sirjan zone, Iran: Implications for reworking of Cadomian arc igneous rocks: Mineralogy and Petrology, v. 111, p. 659–675. doi:10.1007/s00710-016-0490-y

Hoskin, P.W.O., and Black, L.P., 2000, Metamorphic zircon formation by solid-state recrystallization of protolith igneous zircon: Journal of Metamorphic Geology, v. 18, p. 423–439. doi:10.1046/j.1525-1314.2000.00266.x

Hosseini, B., Ahmadi, A., and Ghorbani, M., 2009, April. Metamorphic evolution of the Toutak complex (Sanandaj-Sirjan Zone, Iran), *in* EGU General Assembly Conference Abstracts, v. 11, p. 1077.

Hosseiny, M., 1999, Geological map of Ghorveh: No. 5560: Geological Survey of Iran, Scale 1:100000.

Hunziker, D., Burg, J.P., Bouilhol, P., and Quadt, A., 2015, Jurassic rifting at the Eurasian Tethys margin: Geochemical and geochronological constraints from granitoids of North Makran, southeastern Iran: Tectonics, v. 34, p. 571–593. doi:10.1002/2014TC003768

Ishizuka, O., Tani, K., Reagan, M.K., Kanayama, K., Umino, S., Harigane, Y., Sakamoto, I., Miyajima, Y., Yuasa, M., and Dunkley, D.J., 2011, The timescales of subduction initiation and subsequent evolution of an oceanic island arc: Earth and Planetary Science Letters, v. 306, p. 229–240. doi:10.1016/j.epsl.2011.04.006

Izadyar, J., Mousavizadeh, M., and Eram, M., 2013, Metamorphic evolution of high-pressure Quartz Schists in the Chadegan metamorphic complex, Sanandaj-Sirjan zone, Iran: Geopersia, v. 3, p. 1–20.

Jackson, S.E., Pearson, N.J., Griffin, W.L., and Belousova, E.A., 2004, The application of laser ablation-inductively coupled plasma-mass spectrometry to in situ U–Pb zircon geochronology: Chemical Geology, v. 211, p. 47–69. doi:10.1016/j.chemgeo.2004.06.017

Jenner, F.E., and O'Neill, H.S.C., 2012, Analysis of 60 elements in 616 ocean floor basaltic glasses: Geochemistry, Geophysics, Geosystems, v. 13, p. Q02005. doi:10.1029/2011GC004009

Jung, S., Vieten, K., Romer, R.L., Mezger, K., Hoernes, S., and Satir, M., 2012, Petrogenesis of Tertiary alkaline magmas in the Siebengebirge, Germany: Journal of Petrology, v. 53, p. 2381–2409. doi:10.1093/petrology/egs047

Kampunzu, A.B., and Mohr, F., 1991, Magmatic evolution and petrogenesis in the East African rift system, *in* Kampunzu, A. B., and Lubala, R.T., eds., Magmatism in extensional structural settings – The Phanerozoic African Plate: Heidelberg, Springer Verlag, p. 85–136. doi:10.1007/978-3-642-73966-8_5

Kazmin, V.G., Sbortshikov, I.M., Ricou, L.E., Zonenshain, L.P., Boulin, J., and Knipper, A.L., 1986, Volcanic belts as markers of the Mesozoic-Cenozoic active margin of Eurasia: Tectonophysics, v. 123, p. 123–152. doi:10.1016/0040-1951(86)90195-2

Lashkevitsch, Z.M., Medvedev, A.P., and Krupskiy, Y.Z., 1995, Tectonomagmatic evolution of Carpathians (in Russian): Kiev, Naukova Dumka. P. 1–113.

Le Maitre, R.W., Streckeisen, A., Zanettin, B., Le Bas, M.J., Bonin, B. and Bateman, P. eds., 2002. Igneous rocks: a classification and glossary of terms: recommendations of the International Union of Geological Sciences Subcommission on the Systematics of Igneous Rocks. Cambridge University Press.

Lewandowski, M., Krobicki, M., Matyja, B.A. and Wierzbowski, A., 2003. New paleomagnetic data from Mid-Jurassic to Early Cretaceous sequence of the Eastern Pieniny Klippen Belt (Western Ukraine). In *EGS-AGU-EUG Joint Assembly*. abstract id. 2491

Li, X.W., Mo, X.X., Yu, X.H., Ding, Y., Huang, X.F., Wei, P., and He, W.Y., 2013, Geochronological, geochemical and Sr–Nd–Hf isotopic constraints on the origin of the Cretaceous intraplate volcanism in West Qinling, Central China: Implications for asthenosphere–Lithosphere interaction: Lithos, v. 177, p. 381–401. doi:10.1016/j.lithos.2013.05.020

Li, Z.X., Bogdanova, S.V., Collins, A.S., Davidson, A., De Waele, B., Ernst, R.E., Fitzsimons, I.C.W., Fuck, R.A., Gladkochub, D.P., Jacobs, J., and Karlstrom, K.E., 2008, Assembly, configuration, and break-up history of Rodinia: A synthesis: Precambrian Research, v. 160, p. 179–210. doi:10.1016/j.precamres.2007.04.021

Lucin´ska-Anczkiewicz, A., S´la˛czka, A., Villa, I.M., and Anczkiewicz, R., 2000, $^{39}Ar/^{40}Ar$ dating of the teschenite association rocks from the polish outer Carpathians: Special Paper-Mineralogical Society of Poland, v. 17, p. 241–242.

Ludwig, K.R., 2012, Isoplot, a geochronological toolkit for Microsoft Excel: Berkeley Geochronology Center, Special Publication, v. 5, p. 75.

Maanijou, M., Aliani, F., and Miri, M., 2011, Geochemistry and petrology of granophyric granite veins penetrated in the igneous intrusive complex in south of Qorveh Area, west Iran: Australian Journal of Basic and Applied Sciences, v. 5, p. 926–934. (ISSN 1991–8178).

Mahmoudi, S., Corfu, F., Masoudi, F., Mehrabi, B., and Mohajjel, M., 2011, U–Pb dating and emplacement history of granitoid plutons in the northern Sanandaj–Sirjan Zone, Iran: Journal of Asian Earth Sciences, v. 41, p. 238–249. doi:10.1016/j.jseaes.2011.03.006

Malek-Mahmoudi, F., Davoudian, A.R., Shabanian, N., Azizi, H., Asahara, Y., Neubauer, F., and Dong, Y., 2017, Geochemistry of metabasites from the North Shahrekord metamorphic complex, Sanandaj-Sirjan Zone: Geodynamic implications for the Pan-African basement in Iran: Precambrian Research, v. 293, p. 56–72. doi:10.1016/j.precamres.2017.03.003

Mayer, B., Jung, S., Romer, R.L., Stracke, A., Haase, K.M., and Garbe-Schönberg, C.D., 2013, Petrogenesis of Tertiary hornblende-bearing lavas in the Rhön, Germany: Journal of Petrology, v. 54, p. 2095–2123. doi:10.1093/petrology/egt042

Mazhari, S.A., Bea, F., Amini, S., Ghalamghash, J., Molina, J.F., Montero, P., Scarrow, J.H., and Williams, I.S., 2009, The Eocene bimodal Piranshahr massif of the Sanandaj–Sirjan Zone, NW Iran: A marker of the end of the collision in the Zagros orogeny: Journal of the Geological Society, v. 166, p. 53–69. doi:10.1144/0016-76492008-022

McDonough, W.F., and Sun, S.S., 1995, The composition of the Earth: Chemical Geology, v. 120, p. 223–253. doi:10.1016/0009-2541(94)00140-4

Miyashiro, A., and Shido, F., 1975, Tholeiitic and calc-alkalic series in relation to the behaviors of titanium, vanadium, chromium, and nickel: American Journal of Science, v. 275, p. 265–277. doi:10.2475/ajs.275.3.265

Moghadam, H.S., Khademi, M., Hu, Z., Stern, R.J., Santos, J.F., and Wu, Y., 2015, Cadomian (Ediacaran–Cambrian) arc magmatism in the ChahJam–Biarjmand metamorphic complex (Iran): Magmatism along the northern active margin of Gondwana: Gondwana Research, v. 27, p. 439–452. doi:10.1016/j.gr.2013.10.014

Moghadam, H.S., Li, X.H., Stern, R.J., Santos, J.F., Ghorbani, G., and Pourmohsen, M., 2016, Age and nature of 560–520 Ma calc-alkaline granitoids of Biarjmand, northeast Iran: Insights into Cadomian arc magmatism in northern Gondwana: International Geology Review, v. 58, p. 1492–1509. doi:10.1080/00206814.2016.1166461

Moghadam, H.S., and Stern, R.J., 2015, Ophiolites of Iran: Keys to understanding the tectonic evolution of SW Asia: (II) Mesozoic ophiolites: Journal of Asian Earth Sciences, v. 100, p. 31–59. doi:10.1016/j.jseaes.2014.12.016

Mohajjel, M., and Fergusson, C.L., 2000, Dextral transpression in Late Cretaceous continental collision, Sanandaj–Sirjan zone, western Iran: Journal of Structural Geology, v. 22, p. 1125–1139. doi:10.1016/S0191-8141(00)00023-7

Mohajjel, M., and Fergusson, C.L., 2014, Jurassic to Cenozoic tectonics of the Zagros Orogen in northwestern Iran: International Geology Review, v. 56, p. 263–287. doi:10.1080/00206814.2013.853919

Mohajjel, M., Fergusson, C.L., and Sahandi, M.R., 2003, Cretaceous–Tertiary convergence and continental collision, Sanandaj–Sirjan zone, western Iran: Journal of Asian Earth Sciences, v. 21, p. 397–412. doi:10.1016/S1367-9120(02)00035-4

Moinevaziri, H., Akbarpour, A., and Azizi, H., 2015, Mesozoic magmatism in the northwestern Sanandaj–Sirjan zone as an evidence for active continental margin: Arabian Journal of Geosciences, v. 8, p. 3077–3088. doi:10.1007/s12517-014-1309-y

Mousivand, F., Rastad, E., Meffre, S., Peter, J.M., Mohajjel, M., Zaw, K., and Emami, M.H., 2012, Age and tectonic setting of the Bavanat Cu–Zn–Ag Besshi-type volcanogenic massive sulfide deposit, southern Iran: Mineralium Deposita, v. 47, p. 911–931. doi:10.1007/s00126-012-0407-6

Nasr-Esfahani, A.K., 2012, Tectonic setting of metabasites of the Neo-Tethyan oceanic remains in Sanandaj-Sirjan structural zone, west of Isfahan, central Iran: Islam. Azad Univ. Mashhad Branch, v. 4, p. 75–84.

Nasr-Esfahani, A.K., and Ziaei, H.R., 2007, Using multivariable statistical methods to separation and detection of lithologic units in ETM+ satellite images, case study: Outcrops in the south of Ab-Poneh village, Tiran (west Isfahan): Islamic Azad University Mashhad Branch, v. 17, p. 27–42.

Pearce, J.A., 2008, Geochemical fingerprinting of oceanic basalts with applications to ophiolite classification and the search for Archean oceanic crust: Lithos, v. 100, p. 14–48. doi:10.1016/j.lithos.2007.06.016

Pearce, J.A., Stern, R.J., Bloomer, S.H., and Fryer, P., 2005, Geochemical mapping of the Mariana arc-basin system: Implications for the nature and distribution of subduction components: Geochemistry, Geophysics, Geosystems, v. 6, p. Q07006. doi:10.1029/2004GC000895

Peate, D.W., 1997, The parana-etendeka province: Geophysical Monograph-American Geophysical Union, v. 100, p. 217–246. doi:10.1029/GM100p0217

Peccerillo, A., and Taylor, S.R., 1976, Geochemistry of Eocene calc-alkaline volcanic rocks from the Kastamonu area, northern Turkey: Contributions to Mineralogy and Petrology, v. 58, p. 63–81. doi:10.1007/BF00384745

Philpotts, A., and Ague, J., 2009, Principles of igneous and metamorphic petrology: Cambridge University Press, p. 644.

Pichavant, M., and Macdonald, R., 2007, Crystallization of primitive basaltic magmas at crustal pressures and genesis of the calc-alkaline igneous suite: Experimental evidence from St Vincent, Lesser Antilles arc: Contributions to Mineralogy and Petrology, v. 154, p. 535–558. doi:10.1007/s00410-007

Qin, K.Z., Su, B.X., Sakyi, P.A., Tang, D.M., Li, X.H., Sun, H., Xiao, Q.H., and Liu, P.P., 2011, SIMS zircon U-Pb geochronology and Sr-Nd isotopes of Ni-Cu-Bearing Mafic-Ultramafic intrusions in Eastern Tianshan and Beishan in correlation with flood basalts in Tarim Basin (NW China): Constraints on a ca. 280 Ma mantle plume: American Journal of Science, v. 311, p. 237–260. doi:10.2475/03.2011.03

Rajabzadeh, A.M., and Esmaeili, S., 2014, Investigation on protolith and tectonic setting of metamorphic rocks in the Surian complex using petrographic and geochemical data: Petrology, v. 5, p. 2228–5210. (*(in Persian)*).

Reagan, M.K., Ishizuka, O., Stern, R.J., Kelley, K.A., Ohara, Y., Blichert Toft, J., Bloomer, S.H., Cash, J., Fryer, P., Hanan, B.B., Hickey-Vargas, R., Ishii, T., Kimura, J.I., Peate, D.W., Rowe, M. C., and Woods, M., 2010, Fore-arc basalts and subduction initiation in the Izu– Bonin–Mariana system: Geochemistry, Geophysics, Geosystems, v. 11, p. Q03X12. doi:10.1029/2009GC002871

Redman, B.A., and Keays, R.R., 1985, Archaean basic volcanism in the eastern Goldfields province, Yilgarn Block, western Australia: Precambrian Research, v. 30, p. 113–152. doi:10.1016/0301-9268(85)90048-8

Rogers, N.W., 2006, Basaltic magmatism and the geodynamics of the East African Rift System: Geological Society. London, Special Publications. v. 259, p. 77–93. doi:10.1144/GSL.SP.2006.259.01.08

Rossetti, F., Monié, P., Nasrabady, M., Theye, T., Lucci, F., and Saadat, M., 2017, Early carboniferous subduction-zone metamorphism preserved within the Palaeo-Tethyan Rasht ophiolites (western Alborz, Iran): Journal of the Geological Society, v. 174, p. 741–758. doi:10.1144/jgs2016-130

Saunders, A.D., Storey, M., Kent, R.W., and Norry, M.J., 1992, Consequences of plume-lithosphere interactions: Geological Society. London, Special Publications. v. 68, p. 41–60. doi:10.1144/GSL.SP.1992.068.01.04

Saunders, A.D., and Tarney, J., 1984, Geochemical characteristics of basaltic volcanism within back-arc basins: Geological Society. London, Special Publications. v. 16, p. 59–76. doi:10.1144/GSL.SP.1984.016.01.05

Sepahi, A.A., 2008, Typology and petrogenesis of granitic rocks in the Sanandaj-Sirjan metamorphic belt, Iran: With emphasis on the Alvand plutonic complex: Neues Jahrbuch für Geologie und Paläontologie-Abhandlungen, v. 247, p. 295–312. doi:10.1127/0077-7749/2008/0247-0295

Sepahi, A.A., and Athari, S.F., 2006, Petrology of major granitic plutons of the northwestern part of the Sanandaj-Sirjan metamorphic Belt, Zagros Orogen, Iran: With emphasis on A-type granitoids from the SE Saqqez area. Neues Jahrbuch für Mineralogie-Abhandlungen: Journal of Mineralogy and Geochemistry, v. 183, p. 93–106. doi:10.1127/0077-7757/2006/0063

Shabanian, N., Davoudian, A.R., Dong, Y., and Liu, X., 2017, U-Pb zircon dating, geochemistry and Sr-Nd-Pb isotopic ratios from Azna-Dorud Cadomian metagranites, Sanandaj-Sirjan Zone of Western Iran: Precambrian Research, v. 306, p. 41–60. doi:10.1016/j.precamres.2017.12.037

Shabanian, N., Khalili, M., Davoudian, A.R., and Mohajjel, M., 2009, Petrography and geochemistry of mylonitic granite from Ghaleh-Dezh, NW Azna, Sanandaj-Sirjan zone, Iran. Neues Jahrbuch für Mineralogie-Abhandlungen: Journal of Mineralogy and Geochemistry, v. 185, p. 233–248. doi:10.1127/0077-7757/2009/0121

Shahbazi, H., Salami, S., and Siebel, W., 2014, Genetic classification of magmatic rocks from the Alvand plutonic complex, Hamedan, western Iran, based on zircon crystal morphology: Chemie der Erde-Geochemistry, v. 74, p. 577–584. doi:10.1016/j.chemer.2013.11.001

Shahbazi, H., Siebel, W., Pourmoafee, M., Ghorbani, M., Sepahi, A.A., Shang, C.K., and Abedini, M.V., 2010, Geochemistry and U–Pb zircon geochronology of the Alvand plutonic complex in Sanandaj–Sirjan Zone (Iran): New evidence for Jurassic magmatism: Journal of Asian Earth Sciences, v. 39, p. 668–683. doi:10.1016/j.jseaes.2010.04.014

Shaikh Zakariaei, S.J., and Monsef, I., 2010, Mineralogy-petrofabric of metamorphic rocks in Ghorveh (northwest of Iran): Islamic Azad University Mashhad Branch, v. 77, p. 203–220. (*in Persian*). Iran.

Shakerardakani, F., Neubauer, F., Liu, X., Bernroider, M., Monfaredi, B., and Von Quadt, A., 2018, Tectonic significance of Triassic mafic rocks in the June Complex, Sanandaj–Sirjan zone, Iran: Swiss Journal of Geosciences, v. 111, p. 13–33. doi:10.1007/s00015-017-0281-4

Sheikholeslami, M.R., Pique, A., Mobayen, P., Sabzehei, M., Bellon, H., and Emami, M.H., 2008, Tectono-metamorphic evolution of the Neyriz metamorphic complex, Quri-kor-e-sefid area (Sanandaj-Sirjan Zone, SW Iran): Journal of Asian Earth Sciences, v. 31, p. 504–521. doi:10.1016/j.jseaes.2007.07.004

Shervais, J.W., 1982, Ti-V plots and the petrogenesis of modern and ophiolitic lavas: Earth and Planetary Science Letters, v. 59, p. 101–118. doi:10.1016/0012-821X(82)90120-0

Shinjo, R., Chung, S.-L., Kato, Y., and Kimura, M., 1999, Geochemical and Sr–Nd isotopic characteristics of volcanic rocks from the Okinawa Trough and Ryukyu arc: Implications for the evolution of a young, intracontinental back arc basin: Journal of Geophysical Research: Solid Earth, v. 104, p. 10591–10608. doi:10.1029/1999JB900040

Song, X.Y., Xie, W., Deng, Y.F., Crawford, A.J., Zheng, W.Q., Zhou, G.F., Deng, G., Cheng, S.L., and Li, J., 2011, Slab break-off and the formation of Permian mafic–Ultramafic intrusions in southern margin of Central Asian Orogenic Belt, Xinjiang, NW China: Lithos, v. 127, p. 128–143. doi:10.1016/j.lithos.2011.08.011

Stacey, J.T., and Kramers, J.D., 1975, Approximation of terrestrial lead isotope evolution by a two-stage model: Earth and Planetary Science Letters, v. 26, p. 207–221. doi:10.1016/0012-821X(75)90088-6

Stern, R.J., Fouch, M.J., and Klemperer, S., 2003, An overview of the Izu–Bonin–Mariana subduction factory, *in* Eiler, J., ed., Inside the subduction factory: American Geophysical Union, Geophysical Monograph, v. 138, p. 175–222. doi:10.1029/138GM10. AGU publication, Washington DC, USA.

Stöcklin, J., 1968, Structural history and tectonics of Iran, a review: American Association of Petroleum Geologists, v. 52, p. 1229–1258.

Stöcklin, J., and Nabavi, M.H., 1973, Tectonic map of Iran: Geology Survey Iran. Iran.

Sun, S.S., and McDonough, W.S., 1989, Chemical and isotopic systematics of oceanic basalts: Implications for mantle composition and processes: Geological Society of London. Special Publication, v. 42, p. 313–345. doi:10.1144/GSL.SP.1989.042.01.19

Tanaka, T., Togashi, S., Kamioka, H., Amakawa, H., Kagami, H., Hamamoto, T., Yuhara, M., Orihashi, Y., Yoneda, S., Shimizu, H., Kunimaru, T., Takahashi, K., Yanagi, T., Nakano, T., Fujimaki, H., Shinjo, R., Asahara, Y., Tanimizu, M., and Dragusanu, C., 2000, JNdi-1: A neodymium isotopic reference in consistency with LaJolla neodymium: Chemical Geology, v. 168, p. 279–281. doi:10.1016/S0009-2541(00)00198-4

Tatsumi, Y., 2005, The subduction factory: How it operates in the evolving Earth: GSA Today, v. 15, p. 4. doi:10.1130/1052-5173(2005)015<4:TSFHIO>2.0.CO;2

Thirlwall, M.F., Upton, B.G.J., and Jenkins, C., 1994, Interaction between continental lithosphere and the Iceland plume—Sr–Nd–Pb isotope chemistry of Tertiary basalts, NE Greenland: Journal of Petrology, v. 35, p. 839–879. doi:10.1093/petrology/35.3.839

Tian, W., Campbell, I.H., Allen, C.M., Guan, P., Pan, W., Chen, M., Yu, H., and Zhu, W., 2010, The Tarim picrite–Basalt–Rhyolite suite, a Permian flood basalt from northwest China with contrasting rhyolites produced by fractional crystallization and anatexis: Contributions to Mineralogy and Petrology, v. 160, p. 407–425. doi:10.1007/s00410-009-0485-3

Torkian, A., Khalili, M., and Sepahi, A.A., 2008, Petrology and geochemistry of the I-type calc-alkaline Qorveh Granitoid Complex, Sanandaj-Sirjan Zone, western Iran. Neues Jahrbuch für Mineralogie-Abhandlungen: Journal of Mineralogy and Geochemistry, v. 185, p. 131–142. doi:10.1127/0077-7757/2008/0114

Vidal, P., Deniel, C., Vellutini, P.J., Piguet, P., Coulon, C., Vincent, J., and Audin, J., 1991, Changes of mantle sources in the course of a rift evolution: The Afar case: Geophysical Research Letters, v. 18, no. 10, p. 1913–1916. doi:10.1029/91GL02006

Volker, F., Altherr, R., Jochum, K.P., and McCulloch, M.T., 1997, Quaternary volcanic activity of the southern Red Sea: New data and assessment of models on magma sources and Afar plume-lithosphere interaction: Tectonophysics, v. 278, p. 15–29. doi:10.1016/S0040-1951(97)00092-9

Whitney, D.L., and Evans, B.W., 2010, Abbreviations for names of rock forming minerals: American Mineralogist, v. 95, p. 185–277. doi:10.2138/am.2010.3371

Willbold, M., and Stracke, A., 2006, Trace element composition of mantle end-members: Implications for recycling of oceanic and upper and lower continental crust: Geochemistry Geophysics Geosystems, v. 7, p. Q04004. doi:10.1029/2005GC001005

Xia, L.Q., Li, X.M., Xia, Z.C., Xu, X.Y., Ma, Z.P., and Wang, L.S., 2006, Carboniferous-Permian rift-related volcanism and mantle plume in the Tianshan, northwestern China: Northwestern Geology, v. 39, p. 1–49.

Xu, Y., Chung, S.L., Jahn, B.M., and Wu, G., 2001, Petrologic and geochemical constraints on the petrogenesis of Permian–

Triassic Emeishan flood basalts in southwestern China: Lithos, v. 58, p. 145–168. doi:10.1016/S0024-4937(01)00055-X

Xu, Y.G., He, B., Chung, S.L., Menzies, M.A., and Frey, F.A., 2004, Geologic, geochemical, and geophysical consequences of plume involvement in the Emeishan flood-basalt province: Geology, v. 32, p. 917–920. doi:10.1130/G20602.1

Yajam, S., Ghalamghash, J., Montero, P., Scarrow, J.H., Razavi, S.M.H., and Bea, F., 2015, The spatial and compositional evolution of the Late Jurassic Ghorveh-Dehgolan plutons of the Zagros Orogen, Iran: Geologica Acta: An International Earth Science Journal, v. 13, p. 25–43. doi:10.1344/GeologicaActa2015.13.1.2

Yang, S.F., Li, Z., Chen, H., Santosh, M., Dong, C.W., and Yu, X., 2007, Permian bimodal dyke of Tarim Basin, NW China: Geochemical characteristics and tectonic implications. Gondwana Research, v. 12, p. 113–120. doi:10.1016/j.gr.2006.10.018

Zarasvandi, A., Rezaei, M., Lentz, D., Pourkaseb, H., and Karevani, M., 2015, The Kasian volcanic rocks, Khorramabad, Iran: Evidence for a Jurassic Intra-Oceanic island arc in Neo-Tethys Ocean: Islamic Azad University Mashhad Branch, v. 39, p. 165–178.

Zhang, H., Chen, J., Yang, T., Hou, Z., and Aghazadeh, M., 2018, Jurassic granitoids in the northwestern Sanandaj–Sirjan zone: Evolving magmatism in response to the development of a Neo-Tethyan slab window: Gondwana Research. doi:10.1016/j.gr.2018.01.012

Zhang, H.F., Sun, M., Zhou, X.H., Zhou, M.F., Fan, W.M., and Zheng, J.P., 2003, Secular evolution of the lithosphere beneath the eastern North China Craton: Evidence from Mesozoic basalts and high-Mg andesites: Geochimica et Cosmochimica Acta, v. 67, p. 4373–4387. doi:10.1016/S0016-7037(03)00377-6

Zhang, J.E., Xiao, W., Han, C., Mao, Q., Ao, S., Guo, Q., and Ma, C., 2011, A Devonian to Carboniferous intra-oceanic subduction system in Western Junggar, NW China: Lithos, v. 125, p. 592–606. doi:10.1016/j.lithos.2011.03.013

Zhou, M.F., Zhao, J.H., Jiang, C.Y., Gao, J.F., Wang, W., and Yang, S.H., 2009, OIB-like, heterogeneous mantle sources of Permian basaltic magmatism in the western Tarim Basin, NW China: Implications for a possible Permian large igneous province: Lithos, v. 113, p. 583–594. doi:10.1016/j.lithos.2009.06.027